INTERDISCIPLINARY MATHEMATICS INSTITUTE

2014:07

A 3D Hydrodynamic Model for Heterogeneous Biofilms with Antimicrobial Persistence

Jia Zhao and Qi Wang

PREPRINT SERIES

Report Documentation Page	*Form Approved* *OMB No. 0704-0188*

Public reporting burden for the collection of information is estimated to average 1 hour per response, including the time for reviewing instructions, searching existing data sources, gathering and maintaining the data needed, and completing and reviewing the collection of information Send comments regarding this burden estimate or any other aspect of this collection of information, including suggestions for reducing this burden, to Washington Headquarters Services, Directorate for Information Operations and Reports, 1215 Jefferson Davis Highway, Suite 1204, Arlington VA 22202-4302 Respondents should be aware that notwithstanding any other provision of law, no person shall be subject to a penalty for failing to comply with a collection of information if it does not display a currently valid OMB control number

1. REPORT DATE **2014**	2. REPORT TYPE	3. DATES COVERED **00-00-2014 to 00-00-2014**
4. TITLE AND SUBTITLE **A 3D Hydrodynamic Model for Heterogeneous Biofilms with Antimicrobial Persistence**		5a. CONTRACT NUMBER
		5b. GRANT NUMBER
		5c. PROGRAM ELEMENT NUMBER
6. AUTHOR(S)		5d. PROJECT NUMBER
		5e. TASK NUMBER
		5f. WORK UNIT NUMBER
7. PERFORMING ORGANIZATION NAME(S) AND ADDRESS(ES) **University of South Carolina,Interdisciplinary Mathematics Institute,Columbia,SC,29208**		8. PERFORMING ORGANIZATION REPORT NUMBER
9. SPONSORING/MONITORING AGENCY NAME(S) AND ADDRESS(ES)		10. SPONSOR/MONITOR'S ACRONYM(S)
		11. SPONSOR/MONITOR'S REPORT NUMBER(S)

12. DISTRIBUTION/AVAILABILITY STATEMENT
Approved for public release; distribution unlimited

13. SUPPLEMENTARY NOTES

14. ABSTRACT

Biofilms are known to be more persistent to antimicrobial treatment than planktonic bacterial cells. In addition to the protective extracellular matrix formed primarily by expopolysaccharides (EPS), one of the current point of views on this issue is that there may exist a small portion of phenotypic bacterial variants, known as persisters, which are invulnerable to antimicrobial agents, while the majority of the bacterial cells is susceptible to antimicrobial agents. In this paper, a 3D hydrodynamic model for spatially heterogeneous biofilms based on the phase field formulation is proposed and applied to analyze the mechanism of antimicrobial persistence of biofilms by acknowledging the existence of persisters and susceptible cells in the total population of bacteria. A numerical scheme is devised to solve the model consisting of partial differential equations, which is implemented on graphic processing units (GPUs) for high performance computing, in 3-D space and time. Antimicrobial treatment in an infinitely long quiescent water channel and in a short water tube under inflow and outflow boundary conditions are simulated using the new model, in which multiple dosing locations and strategies are investigated. The model demonstrates the internal spatial and temporal distribution of bacteria, EPS, nutrient and antimicrobial agents, providing a useful tool for analyzing the mechanism of biofilm persistence to antimicrobial agents in an aqueous environment. The numerical result also confirms that the periodic dosing strategy is more effective than the constant dosing strategy in disinfecting biofioms.

15. SUBJECT TERMS					
16. SECURITY CLASSIFICATION OF:			17. LIMITATION OF ABSTRACT	18. NUMBER OF PAGES	19a. NAME OF RESPONSIBLE PERSON
a REPORT **unclassified**	b ABSTRACT **unclassified**	c THIS PAGE **unclassified**	**Same as Report (SAR)**	**41**	

A 3D Hydrodynamic Model for Heterogeneous Biofilms with Antimicrobial Persistence

Jia Zhao*and Qi Wang†

Abstract

Biofilms are known to be more persistent to antimicrobial treatment than planktonic bacterial cells. In addition to the protective extracellular matrix formed primarily by expopolysaccharides (EPS), one of the current point of views on this issue is that there may exist a small portion of phenotypic bacterial variants, known as persisters, which are invulnerable to antimicrobial agents, while the majority of the bacterial cells is susceptible to antimicrobial agents. In this paper, a 3D hydrodynamic model for spatially heterogeneous biofilms based on the phase field formulation is proposed and applied to analyze the mechanism of antimicrobial persistence of biofilms by acknowledging the existence of persisters and susceptible cells in the total population of bacteria. A numerical scheme is devised to solve the model consisting of partial differential equations, which is implemented on graphic processing units (GPUs) for high performance computing, in 3-D space and time. Antimicrobial treatment in an infinitely long quiescent water channel and in a short water tube under inflow and outflow boundary conditions are simulated using the new model, in which multiple dosing locations and strategies are investigated. The model demonstrates the internal spatial and temporal distribution of bacteria, EPS, nutrient and antimicrobial agents, providing a useful tool for analyzing the mechanism of biofilm persistence to antimicrobial agents in an aqueous environment. The numerical result also confirms that the periodic dosing strategy is more effective than the constant dosing strategy in disinfecting biofioms.

1 Introduction

In nature, as long as bacteria colonize on moisture surfaces, biofilms will likely form, which are consisted of the micro-organisms aggregated by bacteria colonies along with their self-produced, glue-like polysacharride matrix, known as the extracellular polymeric substance (EPS). It's commonly perceived by the medical community that biofilms are responsible for many diseases or ailments associated with chronic infections, evidenced by the survey that biofilms are present on the removed tissue of 80% of patients undergoing surgery for chronic sinusitis [36]. Unlike a planktonic bacterium, biofilms are always hard to be eradicated by the standard antimicrobial treatment [28], which perhaps explains the frequent relapse of chronic diseases or ailments associated with biofilms.

Thus, an understanding of the mechanism that underlies biofilm persistence to antimicrobial agents can greatly enhance therapeutic treatment of diseases related with biofilms. Intensive research efforts have been carried out, primarily experimental, to try to understand biofilm dynamics, yet little is fully known. Readers may refer to the review papers [12] and [28] for overviews of current advances in the treatment of biofilms. What is known to us via experimental evidence is that not only one, but many factors can contribute to the biofilm-antimicrobial agent interaction. Among them, one essential factor

---

*Department of Mathematics, University of South Carolina, Columbia, SC 29208

†Department of Mathematics, University of South Carolina, Columbia, SC 29208; Beijing Computational Science Research Center, Beijing, 100083, China; School of Mathematics, Nankai University, Tianjin 300071, China.

is the existence of persister cells within the biofilm colony, which are consisted of a small portion of dormant bacterial variants and are highly tolerant to antimicrobial agents [3]. Contrasting to persister cells, the other bacteria are collectively called susceptible bacteria.

From the clinical point of view, understanding the mechanism of persister formation would be essential for biofilm control and thereby impact on the treatment of diseases responsible by biofilms. For review papers on mechanisms underlying the persister formation, readers are referred to the works by Kim Lewis [28] and [27]. As dormant variants of regular bacterial cells, which doesn't undergo genetic changes, it is convinced that persisters are converted from regular cells due to stresses [3], such as nutrient depletion [5], hydrodynamical shear, existence of antimicrobial agents [33] and so on. Later, when the environment is tolerable, say nutrient is sufficient or the concentration of antimicrobial agents drops under a certain threshold value, biofilms can relapse [6], which implies that persisters convert back into susceptible bacteria for regrowth.

Factoring in persister formation, people have conducted research on therapeutic treatment of diseases induced by biofilms. The review paper [39] provides some information about control strategies for biofilms. Concerning dosing strategies of antimicrobial agents, there exists an evidence that a concentrated dose of biocide is more effective than using a prolonged dose of a lower concentration [20]. In addition, dosing by shocks is more effective than dosing in a persistent manner [19]. But to the best of our knowledge, there does not exist any optimal strategies derived for biofilm control or disease treatment caused by biofilms so far. Currently, the environmental impact of biocide or side-effect of antibiotics have become common concerns, which makes the derivation of an optimal strategy even harder.

Besides the formation of persister bacteria, extra cellular substances (EPS) also play a role in the failure of antimicrobial treatment of biofilms. Basically, EPS is believed to act as a protective barrier to prevent the antimicrobial agents from penetrating deep into the biofilm region, either by reacting with antimicrobial agents [38] or by simply slowing down the diffusion rate via its densely distributed network meshes [41]. Readers can find more details about the role of EPS in biofilm structure and function from [17] and [16].

From the mathematical perspective, several models have been proposed trying to interpret experimental observations on biofilm structures and function. For a review of mathematical models of biofilms, interested readers are referred to [25] and [44] for more details. Mathematical models at different length scales have also been devised, i.e., microscopic scale models (agent based models) [1], mesoscopic scale models (kinetic theory models) [45] and macroscopic scale models (continuum theories) [47], based on the specific issue that one was interested in. Recently, modeling biofilms as multiphase complex fluids has emerged as a promising approach to address some complex and intriguing issues associated with biofilm dynamics [46, 47], where bacteria are regarded as colloids and the biofilm as a polymer gel. In such an approach, a complex fluid model can be devised to analyze the structure formation and function of biofilms in a hydrodynamical setting. In this research direction, the work of Wang et al. represents some latest development [47, 48].

On the issue of biofilm persistence to antimicrobial agents, simple mathematical models have also been developed to test certain mechanisms for persister formation based on the experimental evidence that supports the concept of persisters. For instance in [35], the author claims using a simple mathematical model that persister formation can lead to higher bacterial persistence to antimicrobial agents than those grown in plancktonic culture. In [23], a 3D agent-based model for biofilm dynamics under antimicrobial treatment was developed, in which it showed that substrate limitation can contribute to the persistence of biofilms to antimicrobial agents. Cogan has worked on possible mechanisms of persister formation using time-dependent, but spatially homogeneous models recently [8], [11], [26].

Models on dosing strategies for treating diseases caused by biofilms have also been proposed. Cogan discussed effective dosing strategies using simple mathematical models in [8, 26]. In [10], he discussed the effect of periodic disinfection by a one-dimensional mathematical model. In [43], the adaptive re-

sponse to dosing protocols for biofilm control has also been analyzed, which provides some sufficient conditions for eradicating biofilms under the constant dosing approach. In addition, models analyzing other impact factors, which may contribute to biofilm's persistence to antimicrobial agents, have also been proposed. For instance, the author in [13] tried to analyze and simulate diffusive resistance of bacterial biofilms to penetration of antibiotics.

To our best knowledge, there has yet been a mathematical model which takes into account both the hydrodynamic effect and the spatio-temporal heterogeneous structures of biofilms in full three dimension in space and time. However, these factors are important in biofilm structure formation and function, especially, concerning with the biofilm's persistence to antimicrobial agents. In this paper, We develop a full 3-D hydrodynamic model for biofilms of multiple bacterial phenotypes; in particular, we limit the phenotypes to the persister and susceptible type. This model extends our previous model for biofilm-solvent mixture [47] by distinguishing between the persister cell and the susceptible cell when biofilms are treated with antimicrobial agents. In this model, the interplay among the various biomass components such as various bacterial types, EPS and solvent is carefully accounted for both hydrodynamically and chemically so that dead bacteria can be deteriorate into solvent and decomposed into EPS simultaneously some time after their death. Our model shows that the dynamical interaction between these two general phenotypes can impact dramatically on the overall dynamics of the biofilm. The most distinctive attribute of this model is that it provides the spatio-temporal resolution that can resolve more details about antimicrobial action against biofilm colonies in space and time than the previous models can, providing a much needed insight into dynamics of antimicrobial treatment.

The rest of this paper is organized as follows: In section two, we provide the formulation of the hydrodynamic theory for the biofilm system based on the phase field formulation. Then, an efficient numerical solver for this coupled fluid matrix-biofilm partial differential equation system by semi-implicit finite difference strategy is proposed in section three. In section four, numerical simulations and results are presented and discussed. Finally, we summarize the result and draw a conclusion.

2 Mathematical Model Formulation

2.1 Notations

We model the biofilm together with its surrounding aqueous environment as a mixture of complex fluids. The biofilm is consisted of the biomass immersed in solvent; whereas the biomass is made up of bacteria and their products like exopolysaccharide (EPS). Nutrient and antimicrobial agents are small molecule substances dissolved in solvent. Let ϕ_{bs} be the volume fraction of the bacteria that are susceptible to antimicrobial agents, ϕ_{bp} the volume fraction of the bacteria that are persistent to antimicrobial agents, ϕ_{bd} the volume fraction of the dead bacteria, and ϕ_p the volume fraction of EPS. We note that the EPS is the product of the live bacteria at the presence of nutrient. Dead bacteria do not produce any EPS and, over times, dead bacteria can dissolve into solvent and part of them will be released as EPS in the biofilm colony because some EPSs are attached to the cell membrane at the moment when the cell dies. We in addition denote the concentration of the nutrient and the antimicrobial agent as c and d, respectively. To make contact with our previous binary mixture model for biofilms, we define ϕ_n the volume fraction of the biomass, which consists of all the volume fractions for the bacteria ϕ_b as well as EPS ϕ_p, i.e.,

$$\phi_n = \phi_b + \phi_p, \quad \phi_b = \phi_{bs} + \phi_{bp} + \phi_{bd}.$$

In addition to the volume fractions introduced above, the volume fraction of the solvent is denoted as ϕ_s. Due to the small molecular weigh in the nutrient and antimicrobial molecules, we will not explicitly

3

count their mass and volume in this model. The incompressibility of the complex fluid mixture then implies $\phi_s + \phi_n = 1$.

In this model, we make a simplifying assumption that all component in the biomass including the bacteria and EPS share the same mass density. We denote ρ_n and ρ_s the density of biomass and solvent, and $\mathbf{v}_n$ and $\mathbf{v}_s$ the velocity of biomass and solvent, respectively. Then, the volume averaged velocity and density are given respectively by

$$\mathbf{v} = \phi_n \mathbf{v}_n + \phi_s \mathbf{v}_s, \quad \rho = \phi_n \rho_n + \phi_s \rho_s.$$

We assume the bacteria, regardless whether they are live or dead, persisters or susceptibles, and the EPS mix with the solvent owing to the osmotic pressure. Then, we adopt the modified mixing free energy introduced in ([47], [48]) and denote the energy density by f:

$$f = \frac{\gamma_1}{2} k_B T \|\nabla \phi_n\|^2 + \gamma_2 k_B T \left(\frac{\phi_n}{N} \ln \phi_n + (1 - \phi_n) \ln(1 - \phi_n) + \chi \phi_n (1 - \phi_n) \right). \quad (1)$$

This is the modified Flory-Huggins mixing free energy with a conformational entropy added, in which γ_1, γ_2 parametrize the strength of the conformational entropy and bulk mixing free energy, respectively, χ is the mixing parameter, N is the extended polymerization index for the biomass, k_B is the Boltzmann constant and T is the absolute temperature.

2.2 Transport equations for biomass components

Given the mixing free energy density f in (1), the "extended" chemical potentials with respect to each component in the biomass are summarized as follows

$$\mu_{bs} = \frac{\delta f}{\delta \phi_{bs}}, \quad \mu_{bp} = \frac{\delta f}{\delta \phi_{bp}}, \quad \mu_{bd} = \frac{\delta f}{\delta \phi_{bd}}, \quad \mu_p = \frac{\delta f}{\delta \phi_p}.$$

The transport equation for the volume fraction of each biomass component is governed by a reactive Cahn-Hilliard equation,

$$
\begin{aligned}
\frac{\partial}{\partial t} \phi_{bs} + \nabla \cdot (\phi_{bs} \mathbf{v}) &= \nabla \cdot (\lambda_{bs} \phi_{bs} \nabla \mu_{bs}) + g_{bs}, \\
\frac{\partial}{\partial t} \phi_{bp} + \nabla \cdot (\phi_{bp} \mathbf{v}) &= \nabla \cdot (\lambda_{bp} \phi_{bp} \nabla \mu_{bp}) + g_{bp}, \\
\frac{\partial}{\partial t} \phi_{bd} + \nabla \cdot (\phi_{bd} \mathbf{v}) &= \nabla \cdot (\lambda_{bd} \phi_{bd} \nabla \mu_{bd}) + g_{bd}, \\
\frac{\partial}{\partial t} \phi_p + \nabla \cdot (\phi_p \mathbf{v}) &= \nabla \cdot (\lambda_p \phi_p \nabla \mu_p) + g_p,
\end{aligned}
\quad (2)
$$

where g_{bs}, g_{bp}, g_{bd} and g_p are the reactive terms (rates) for the susceptible bacteria, persisters, dead bacteria, and the EPS component, respectively, which will be given in details in the next subsection, λ_{bs}, λ_{bp}, λ_{bd} and λ_p are the motility parameters for the transport of the four components, which can be functions of the biomass volume fractions.

2.3 Transport equations for nutrient and antimicrobial agents

In this model, the nutrient is treated as a phantom material, in which its mass is completely neglected, but the chemical effects are retained. This is because nutrient is consisted of small molecule materials compared to the biomass, which are made up of the bacterial cells and large molecular EPS. Specifically, oxygen is one of the key ingredients in nutrient for the biofilm formation.

4

The governing equation for the nutrient concentration (c) is given by a reaction-convection-diffusion equation with a varying diffusion coefficient and reactive term, namely,

$$\frac{\partial(\phi_s c)}{\partial t} + \nabla \cdot (c\mathbf{v}_s \phi_s) = \nabla \cdot (D_s \phi_s \nabla c) + g_c, \tag{3}$$

where D_s is the diffusion coefficient and g_c is the nutrient consumption term. It was suggested in [40] that

$$\frac{D_{c,polymer}}{D_c} = 0.75,$$

where $D_{c,polymer}$ is the diffusion rate of nutrient in a fully developed biofilm and D_c is the diffusion rate in the pure solvent. In particular, D_c is measured as $2 \times 10^{-9} \ m^{-2}s^{-1}$ at temperature $25\ ^\circ C$ for oxygen. Since the molecular mass of oxygen is relatively small, we propose that it can penetrate the EPS and the membrane of cells equally. Therefore, the diffusion coefficient of oxygen in biofilms can be formulated as

$$D_s = D_c \frac{2(1-\phi_n)}{2+\phi_n},$$

where the second term on the right represents the reduction of the diffusion rate due to the presence of the biomass.

Like the nutrient, an antimicrobial agent can also be modeled as a phantom material. The transport equation of it is proposed as follows

$$\frac{\partial(\phi_s d)}{\partial t} + \nabla \cdot (d\mathbf{v}_s \phi_s) = \nabla \cdot (D_e \phi_s \nabla d) + g_d, \tag{4}$$

where D_e is the diffusion coefficient of the antimicrobial agents and g_d is the reactive term including the antimicrobial injection rate. For some antimicrobial agents, such as the Penicillin, which is of a larger molecule, the biomass (live bacteria and EPS, as well as the dead cells) can prevent the antimicrobial agents from penetrating deeper into the biofilm over times. To quantify this diffusive effect, a comparative study of three cases, by adjusting the diffusion rate of antimicrobial agents, will be conducted in this paper. The simplest case is proposed as follows

$$D_{e1} = D_d, \tag{5}$$

which represents an isotropic diffusion. By considering the fact that the network of EPS and the presence of bacterial cells can slow down the penetration, the second case is proposed as follows

$$D_{e2} = D_d \frac{2(1-\phi_b)}{2+\phi_b} \frac{\phi_s}{\phi_s + \frac{\phi_p}{D_{pr}}}, \tag{6}$$

where D_{pr} is a parameter in the Hinson model [22] fitted experimentally. In the last case, we assume that both EPS and various bacteria in the biofilm can slow down the diffusion of antimicrobial agents at various rates. The diffusion rate is formulated as follows

$$D_{e3} = D_d \frac{2[1-(\phi_{bs}+\phi_{bp})]}{2+\phi_{bs}+\phi_{bp}} \frac{\phi_s}{\phi_s + \frac{\phi_p+\phi_{bd}}{D_{pr}}}. \tag{7}$$

On the right hand side of the formula for D_{e2} and D_{e3}, the second term represents the reduction due to the physical presence of bacteria, and the third term is an empirical fitting, accounting for the reduction effect due to the presence of EPS alone or EPS and dead bacteria combined. We use $D_{pr} = 0.02$ throughout the paper.

2.4 Hydrodynamic equations for the complex fluid mixture

To complete this biological model, the balance equation for the averaged velocity and for the mass density is given below, respectively. For the average velocity $\mathbf{v}$, it's assumed to be solenoidal. Then, the continuity and the momentum balance equations are given, respectively, by

$$\rho(\partial_t \mathbf{v} + \mathbf{v} \cdot \nabla \mathbf{v}) = \nabla \cdot (\phi_b \tau_b + \phi_p \tau_p + \phi_s \tau_s) - [\nabla p + \gamma_1 k_B T \nabla \cdot (\nabla \phi_n \otimes \nabla \phi_n)],$$

$$\nabla \cdot \mathbf{v} = 0,$$

(8)

where p is the hydrostatic pressure, τ_b, τ_p and τ_s are the stress tensor due to bacteria, the EPS, and solvent, respectively. The last term in the momentum equation is due to the spatial inhomogeneity of the biomass distribution, which is derived from the least action principle [47].

In this paper, we are interested in the growth dynamics of the biofilm, whose time scale is significantly larger than the relaxation time scale in the EPS. We therefore model all effective biofilm components as viscous fluids:

$$\tau_b = 2\eta_b \mathbf{D}_n, \quad \tau_p = 2\eta_p \mathbf{D}_n, \quad \tau_s = 2\eta_s \mathbf{D}_s,$$

where η_b, η_p and η_s are the viscosity of bacteria, the EPS and solvent, respectively, which can be functions of volume fractions of the effective biofilm components. Here, the rate of strain tensors for each component is defined respectively by

$$\mathbf{D}_n = \frac{1}{2} \left(\nabla \mathbf{v}_n + \nabla \mathbf{v}_n^T \right), \quad \mathbf{D}_s = \frac{1}{2} \left(\nabla \mathbf{v}_s + \nabla \mathbf{v}_s^T \right),$$

where we assume the rates of strain tensor for the effective biomass components are the same given by $\mathbf{D}_n$.

2.5 Reactive kinetics of biomass components in biofilms

In order to complete this model, we need to propose reactive kinetics for the effective biomass components, for which it is necessary for us to sort out the relations among the various components with respect to their reactive kinetics.

2.5.1 Reactive kinetics of susceptible bacteria and persisters

The bacterial growth depends on the nutrient and the concentration of antimicrobial agents present in the biofilm colony. The two different bacterial phenotypes (susceptible and persister cells) have different growth mechanisms; thus we assume that both the susceptible and the persister cell grow on their own at their own rates, respectively. For both bacterial phenotypes, death rates due to natural causes are taken into account as well. In addition, both susceptible bacteria and persisters can be killed by antimicrobial agents, even though persisters are killed in a much slower rate, due to its antimicrobial persistence. We allow all these features in the model so that they can be turned on and off depending on the time scale that we try to resolve. It is perceived that susceptible bacteria and persisters can be converted mutually, based on the stage of their growth [28] and the surrounding environment [8], such as accessibility to nutrient and antimicrobial agents etc.

The reactive kinetics for these two types of live bacteria are proposed, respectively, as follows:

$$g_{bs} = \frac{C_2 c}{K_1 + c}(1 - \frac{\phi_{bs}}{\phi_{bs,\max}})\frac{\phi_{bs}^2}{\phi_{bs} + \phi_{\min}} - b_{sp}\phi_{bs} + b_{ps}\phi_{bp} - (\frac{r_{bs}K_{sd}^2}{K_{sd}^2 + c^2} + \frac{C_3 d}{K_3 + d})\phi_{bs},$$

$$g_{bp} = \frac{C_4 c}{K_2 + c}(1 - \frac{\phi_{bp}}{\phi_{bp,\max}})\phi_{bp} + b_{sp}\phi_{bs} - b_{ps}\phi_{bp} - (\frac{r_{bp}K_{pd}}{K_{pd} + c} + \frac{C_{12} d}{d + K_3})\phi_{bp},$$

(9)

where C_2 and C_4 are the growth rate for the susceptible and the persister, respectively; $\phi_{bs,\max}, \phi_{bp,\max}$ are the maximum volume fraction for susceptible bacteria and persisters, respectively; b_{sp} and b_{ps} are the conversion rates between the two types of bacteria; r_{bs}, r_{bp} are the natural death rates due to nutrient depletion for susceptible bacteria and persisters, respectively, and C_3, C_{12} are the death rates for susceptible bacteria and persisters due to antimicrobial agents, respectively. $K_1, K_2, K_3, K_{sd}, K_{pd}$ are half saturation constants in the Monod models adopted. We assume $r_{bs} >> r_{bp}$ and $C_3 >> C_{12}$ in the above model. We note the extra term $\frac{\phi_{bs}}{\phi_{bs}+\phi_{\min}}$ in g_{bs} in the susceptible bacterial growth is meant to rule out the effect of planktonic susceptible bacteria in biofilms.

In the following, we propose systematically a formulation for the switch function b_{sp} and b_{ps} between the two types of bacteria, based on the experimental description, as well as literature on mathematical interpretation. It is basically agreed that conversion between the susceptible and the persister is induced by the stress [2], which can be classified into two categories: the stress from exogenous sources, such as antimicrobial treatment, and the stress self-imposed during the bacterial growth, such as starvation. Based on this, we assume the conversion rate b_{sp}, b_{ps} are functions of concentrations of nutrient and antimicrobial agents:

$$b_{sp} = b_{sp}(c, d), \quad b_{ps} = b_{ps}(c, d). \tag{10}$$

For conversion rate b_{sp}, we note that there should be two separate leading order terms, which represent the effect of nutrient and antimicrobial agents, respectively, since these factors represent distinct stresses and conversion occurring at the existence of the stress. For instance, nutrient depletion alone would induce persister formation [31], [5], [6]; without nutrient depletion, persister formation would also be induced in response to the antimicrobial stress [14]. Thus, we propose b_{sp} as follows:

$$b_{sp} = \left(b_{sp1} \frac{k_{spc}^{n_c}}{k_{spc}^{n_c} + c^{n_c}} + b_{sp2} \frac{d^{n_d}}{k_{spd}^{n_d} + d^{n_d}} \right) \left(1 - \frac{\phi_{bp}}{\phi_{bp,\max}} \right), \tag{11}$$

where the first term describes the fact that bacteria turn into dominant persisters due to nutrient depletion [31], the second term depicts the "stress" caused by antimicrobial agents that promotes the conversion [14], and the last term represents the carrying capacity for the persister. Here $b_{sp,1}$ and $b_{sp,2}$ represents the maximum conversion rates from the susceptible to the persister due to nutrient depletion and the antimicrobial agent distribution, respectively. Although it is plausible to propose one more term in b_{sp}, which depends both on nutrient and antimicrobial agents, this correlation is perceived as a high-order term in this model; therefore, we omit it here for simplicity.

For the conversion rate b_{ps}, it is assumed nonzero only if both the nutrient starvation stress and the antimicrobial stress are under certain threshold values. Namely, it should possesses the following properties: it is zero when antimicrobial agents level is high enough, since a biofilm with persisters is tolerable to antimicrobial treatment, and monotonically increases to a constant level as the concentration of antimicrobial agents drops below the threshold value, since biofilms are observed to recover after an antimicrobial treatment. In addition, the availability of nutrient can facilitate this process [6]. One simple rate is thus proposed as follows

$$b_{ps} = b_{ps,\max} \frac{c^{m_c}}{k_{psc}^{m_c} + c^{m_c}} \frac{k_{psd}^{m_d}}{k_{psd}^{m_d} + d^{m_d}}, \tag{12}$$

where $b_{ps,\max}$ is the maximum conversion rate; k_{psc} and k_{psd} are the half-saturation constants, and m_c and m_d are parameters controlling the rate of transition in the switch function.

2.5.2 Reactive kinetics of dead bacteria

Besides the live bacteria, the volume fraction of the dead bacteria is also tracked in this model. It is assumed the dead bacteria stay within the biofilm in the time scale that this model is valid. Meanwhile, we assume some dead bacterial cells are attached to the biofilm acting as EPS while others are converted into solvent due to cell lysis [4] at certain specified rates in the time scale of our interest,

$$g_{bd} = (r_{bs}\frac{K_{sd}^2}{K_{sd}^2 + c^2} + \frac{C_3 d}{K_3 + d})\phi_{bs} + r_{bp}\phi_{bp} - r_{dp}\phi_{bd} - r_{bd}\phi_{bd}, \tag{13}$$

where r_{bs}, r_{bp} are the natural death rates given before, C_3 is the antimicrobial killing rate of susceptible bacteria with the half saturation rate K_3, r_{dp} represents the conversion rate from dead bacteria to EPS, and r_{bd} is due to the decomposition of dead bacteria into solvent.

2.5.3 Reactive kinetics of EPS

EPS is basically produced by susceptible bacteria and persisters as well as converted from dead bacteria. Over the time, EPS can be dissolved into solvent due to reactive effects. So, the growth rate for the EPS is proposed as follows

$$g_p = [\frac{C_5 c}{K_5 + c}\phi_{bs} + \frac{C_6 c}{K_6 + c}\phi_{bp}](1 - C_p\frac{\phi_p}{\phi_{p,\max}}) + r_{dp}\phi_{bd} - r_p\phi_p, \tag{14}$$

where C_5, C_6 are the growth rate of EPS due to susceptible bacteria and persisters, respectively, K_5, K_6 are half saturation constants, $\phi_{p,\max}$ is the maximum volume fraction that EPS can achieve in the biofilm, and r_p represents the dissolving rate of EPS into solvent.

2.5.4 Reactive kinetics of nutrient

We assume the nutrient is consumed by the live bacteria only and the nutrient decay rate is proportional to the bacterial volume fraction:

$$g_c = -C_7(\phi_{bs} + \mu_2\phi_{bp})\frac{c}{K_7 + c}, \tag{15}$$

where μ_2 is a measure of the nutrient consumption efficiency of the persister cells relative to the susceptible cells, K_7 is a saturation constant and C_7 parametrizes the consumption rate of nutrient.

2.5.5 Reactive kinetics of antimicrobial agents

The antimicrobial concentration depends on the live bacterial concentration as well as the EPS concentration. It is "absorbed/consumed" by the live bacteria and possibly diluted by the EPS via chemical reactions. Thus, the presence of both bacteria and EPS can reduce the concentration of antimicrobial agents. We thus propose the decay rate of the antimicrobial agents as follows:

$$g_d = -(C_8\phi_{bs} + C_9\phi_{bp} + C_{10}\phi_{bd} + C_{11}\phi_p)\frac{d}{K_8 + d} + f_d(\mathbf{x}, t) \tag{16}$$

where K_8 is a half saturation constant, C_8 is the decay rate of antimicrobial agents due to the drug-susceptible bacteria interaction, C_9 is the decay rate due to drug-persister cell interaction, and C_{10} is that due to the drug and dead bacterial cell interaction, while C_{11} is that due to drug-EPS interaction. Here

8

f_d is the source term of antimicrobial agents, which represents the injection/supply rate of antimicrobial agents into the biofilm, given by

$$f_d(\mathbf{x}, t) = \frac{1}{\sqrt{\pi\delta}} M(t) e^{-\frac{(\mathbf{x}-\mathbf{x}_0)^2}{\delta}}$$

where $M(t)$ is a nonnegative, periodic function between 0 and M_{max} with periodic T and δ is a small parameter limiting the range of injection in space.

2.6   Boundary Conditions

In this study, we assume the biofilm is confined in a cubic domain: $[0 \quad L_x] \times [0 \quad L_y] \times [0 \quad L_z]$ where L_x, L_y, L_z are the length in the x, y, z direction, respectively. The boundary conditions for the model are proposed based on the physical situation that we intend to simulate. In this paper, we consider two physical settings corresponding to two sets of boundary conditions. One is for a quiescent aqueous long channel and the other is for a short water tube or flow cell with a rectangular cross-section.

2.6.1   Boundary conditions for the long channel

To mimic the biofilm development in a long water channel, both x and z directions are assumed periodic. In the y direction, no-flux boundary conditions are imposed,

$$
\begin{aligned}
[c\mathbf{v}_s\phi_s - D_s\phi_s\nabla c] \cdot \mathbf{n}|_{y=0,L_y} &= 0, \\
[d\mathbf{v}_s\phi_s - D_d\phi_s\nabla d] \cdot \mathbf{n}|_{y=0,L_y} &= 0, \\
\nabla\phi_i \cdot \mathbf{n}|_{y=0,L_y} &= 0, \quad i = bs, bp, bd, p, \\
(\mathbf{v}\phi_i - \lambda\phi_i\nabla\frac{\delta F}{\delta\phi_i}) \cdot \mathbf{n}|_{y=0,L_y} &= 0, \quad i = bs, bp, bd, p.
\end{aligned}
$$

For the average velocity we impose the no-slip condition on the solid walls $\mathbf{v}|_{y=0,L_y} = 0$. We can also impose a nutrient feeding condition $c|_{y=L_y} = c^*$ in place of the zero-flux condition in certain parts of the boundary as needed.

2.6.2   Boundary conditions for the short flow-cell

For the case of biofilms in a short water tube/flow cell, periodic boundary conditions are imposed only in the z direction. The x axis is assumed to align with the inlet-outlet direction. The inlet velocity at $x = 0$ is given by $\mathbf{v}_0 = (p_0y(1-y), 0, 0)$, where p_0 is a prescribed pressure gradient. By assuming that the solvent has already reached a steady state while flowing out of the cell at $x = L_x$, we prescribe $\mathbf{v}_x = 0$ at the outlet end. For the nutrient concentration c, we impose the feeding boundary condition at $x = 0$ as $c = c_0(y)$ and $c_x = 0$ is assumed at $x = L_x$. For the biomass components, we impose no-flux boundary conditions in the x direction,

$$
\begin{aligned}
\nabla\phi_i \cdot \mathbf{n}|_{x=0,L_x} &= 0, \quad i = bs, bp, bd, p, \\
(\mathbf{v}\phi_i - \lambda\phi_i\nabla\frac{\delta f}{\delta\phi_i}) \cdot \mathbf{n}|_{x=0,L_x} &= 0, \quad i = bs, bp, p, bd.
\end{aligned}
$$

We remark that this boundary condition works for a limited time frame before the biomass reaches the boundary. Beyond that moment, it must be modified. In the y direction, we impose no-flux boundary

conditions for nutrient, solvent, antimicrobial agents, and biomass components, respectively,

$$
\begin{aligned}
{[c\mathbf{v}_s\phi_s - D_s\phi_s\nabla c]\cdot\mathbf{n}|_{y=0,L_y}} &= 0, \\
{[d\mathbf{v}_s\phi_s - D_d\phi_s\nabla d]\cdot\mathbf{n}|_{y=0,L_y}} &= 0, \\
\nabla\phi_i\cdot\mathbf{n}|_{y=0,L_y} &= 0, \quad i = bs, bp, bd, p, \\
\left(\mathbf{v}\phi_i - \lambda\phi_i\nabla\frac{\delta f}{\delta\phi_i}\right)\cdot\mathbf{n}|_{y=0,L_y} &= 0, \quad i = bs, bp, bd, p.
\end{aligned}
$$

and the no-slip boundary condition is proposed for the velocity on the solid walls: $\mathbf{v}|_{y=0,L_y} = 0$.

2.7 Nondimensionalization

Let t_0 and h represent the reference time and length scale, respectively. We use these two characteristic scales to nondimensionalize the variables and equations. In this study, we approximate the mobility parameter by a single constant λ. The nondimensional variables are then given by

$$
\begin{gathered}
\tilde{t} = \tfrac{t}{t_0}, \tilde{x} = \tfrac{x}{h}, \tilde{\mathbf{v}} = \tfrac{\mathbf{v}t_0}{h}, \tilde{\tau} = \tfrac{\tau t_0^2}{\rho_0 h^2}, \tilde{p} = \tfrac{pt_0^2}{\rho_0 h^2}, \tilde{c} = \tfrac{c}{c_0}, \tilde{d} = \tfrac{d}{d_0}, \\
\Lambda = \tfrac{\lambda\rho_0}{t_0}, \quad Re_s = \tfrac{\rho_0 h^2}{\eta_s t_0}, \quad \Gamma_1 = \tfrac{\gamma_1 kTt_0^2}{\rho_0 h^4}, \quad \Gamma_2 = \tfrac{\gamma_2 kTt_0^2}{\rho_0 h^2}, \quad \tilde{\rho} = \phi_s\tfrac{\rho_s}{\rho_0} + \phi_n\tfrac{\rho_n}{\rho_0}, \\
\tilde{D}_s = \tfrac{D_s t_0}{h^2}, \quad \tilde{D}_d = \tfrac{D_d t_0}{h^2}, \\
\tilde{C}_i = C_i t_0, i = 1, 2, ..., 11; \tilde{K}_i = \tfrac{K_i}{c_0}, i = 2, 5, 6, 7, spc, psc; \tilde{K}_j = \tfrac{K_j}{d_0}, j = 3, 8, spd, psd \\
\tilde{b}_i = b_i t_0, i = sp1, sp2, psmax; \tilde{r}_i = r_i t_0, i = bs, bp, bd, p.
\end{gathered}
\tag{17}
$$

where c_0, d_0 denote the characteristic substrate concentration of nutrient and antimicrobial agents, respectively.

For simplicity, we drop the symbol of tilde $\tilde{\ }$. The nondimensionalized PDEs governing the biofilm system are summarized as follows:

$$
\left\{
\begin{aligned}
\rho\left(\tfrac{\partial\mathbf{v}}{\partial t} + \mathbf{v}\cdot\nabla\mathbf{v}\right) &= \nabla\cdot(\phi_b\tau_b + \phi_p\tau_p + \phi_s\tau_s) - [\nabla p + \Gamma_1\nabla\cdot(\nabla\phi_n\otimes\nabla\phi_n)], \\[4pt]
\nabla\cdot\mathbf{v} &= 0, \\[4pt]
\tfrac{\partial}{\partial t}\phi_{bs} + \nabla\cdot(\phi_{bs}\mathbf{v}) &= \nabla\cdot(\Lambda\phi_{bs}\nabla\mu_{bs}) + g_{bs}, \\[4pt]
\tfrac{\partial}{\partial t}\phi_{bp} + \nabla\cdot(\phi_{bp}\mathbf{v}) &= \nabla\cdot(\Lambda\phi_{bp}\nabla\mu_{bp}) + g_{bp}, \\[4pt]
\tfrac{\partial}{\partial t}\phi_{bd} + \nabla\cdot(\phi_{bd}\mathbf{v}) &= \nabla\cdot(\Lambda\phi_{bd}\nabla\mu_{bd}) + g_{bd}, \\[4pt]
\tfrac{\partial}{\partial t}\phi_p + \nabla\cdot(\phi_p\mathbf{v}) &= \nabla\cdot(\Lambda\phi_p\nabla\mu_p) + g_p, \\[4pt]
\tfrac{\partial\phi_s c}{\partial t} + \nabla\cdot(c\mathbf{v}_s\phi_s) &= \nabla\cdot(D_s\phi_s\nabla c) + g_c, \\[4pt]
\tfrac{\partial\phi_s d}{\partial t} + \nabla\cdot(d\mathbf{v}_s\phi_s) &= \nabla\cdot(D_e\phi_s\nabla d) + g_d.
\end{aligned}
\right.
\tag{18}
$$

where the reactive terms for each components are given respectively as follows

$$
\begin{cases}
g_{bs} &= \frac{C_2 c}{K_1 + c}(1 - \frac{\phi_{bs}}{\phi_{bs,\max}})\frac{\phi_{bs}^2}{\phi_{bs} + \phi_{\min}} - b_{sp}\phi_{bs} + b_{ps}\phi_{bp} - (\frac{r_{bs}K_{sd}^2}{K_{sd}^2 + c} + \frac{C_3 d}{K_3 + d})\phi_{bs}, \\[2mm]
g_{bp} &= \frac{C_4 c}{K_2 + c}(1 - \frac{\phi_{bp}}{\phi_{bp,\max}})\phi_{bp} + b_{sp}\phi_{bs} - b_{ps}\phi_{bp} - (r_{bp} + \frac{C_{12} d}{d + K_3})\phi_{bp}, \\[2mm]
g_{bd} &= (r_{bs}\frac{K_{sd}^2}{K_{sd}^2 + c^2} + \frac{C_3 d}{K_3 + d})\phi_{bs} + r_{bp}\phi_{bp} - r_{dp}\phi_{bd} - r_{bd}\phi_{bd}, \\[2mm]
g_p &= [\frac{C_5 c}{K_5 + c}\phi_{bs} + \frac{C_6 c}{K_6 + c}\phi_{bp}](1 - C_p\phi_p) + r_{dp}\phi_{bd} - r_p\phi_p, \\[2mm]
g_c &= (\phi_{bs} + \mu_2\phi_{bp})\frac{C_7 c}{K_7 + c}, \\[2mm]
g_d &= -(C_8\phi_{bs} + C_9\phi_{bp} + C_{10}\phi_{bd} + C_{11}\phi_p)\frac{d}{K_8 + d} + \frac{1}{\sqrt{\pi\delta}}M(t)e^{-\frac{(\mathbf{x} - \mathbf{x_0})^2}{\delta}};
\end{cases}
\tag{19}
$$

some of the rates are prescribed specifically as

$$
\begin{aligned}
b_{sp} &= \left(b_{sp1}\frac{k_{spc}^{n_c}}{k_{spc}^{n_c} + c^{n_c}} + b_{sp2}\frac{d^{n_d}}{k_{spd}^{n_d} + d^{n_d}} \right)(1 - \frac{\phi_{bp}}{\phi_{bp,\max}}), \\
b_{ps} &= b_{ps,\max}\frac{c^{m_c}}{k_{psc}^{m_c} + c^{m_c}}\frac{k_{psd}^{m_d}}{k_{psd}^{m_d} + d^{m_d}}.
\end{aligned}
\tag{20}
$$

3   Numerical Methods

We will solve the partial differential equation system, consisting of the governing equations of momentum, continuity, biomass and functional components, numerically in 3D space and time by a semi-implicit, finite difference method. We now discuss its discretization briefly. For simplify, in the following, we use the symbol of over-line for the extrapolated data, $\overline{\mathbf{v}}^{n+1} = 2\mathbf{v}^n - \mathbf{v}^{n-1}$.

Overall, we have 10 coupled PDEs. We solve the momentum equation and continuity equation first by the Gauge-Uzawa method [21]. Recall that the momentum equation is given by

$$
\rho(\frac{\partial \mathbf{v}}{\partial t} + \mathbf{v} \cdot \nabla\mathbf{v}) = \nabla \cdot (\phi_b\tau_b + \phi_p\tau_p + \phi_s\tau_s) - [\nabla p + \Gamma_1\nabla \cdot (\nabla\phi_n \otimes \nabla\phi_n)].
$$

By adding a second order term $-\frac{1}{R_{e_a}}\nabla^2\mathbf{v}$ on both side, it turns into

$$
\rho(\frac{\partial \mathbf{v}}{\partial t} + \mathbf{v} \cdot \nabla\mathbf{v}) - \frac{1}{R_{e_a}}\nabla^2\mathbf{v} = -\nabla p - \Gamma_1\nabla^2\phi_n\nabla\phi_n + \nabla \cdot (\phi_b\tau_b + \phi_p\tau_p + \phi_s\tau_s) - \frac{1}{R_{e_a}}\nabla^2\mathbf{v}, \tag{21}
$$

where R_{e_a} is the averaged Reynolds number, computed by

$$
\frac{1}{R_{e_a}} = \frac{\phi_{b,avg}}{R_{e_b}} + \frac{\phi_{p,avg}}{R_{e_p}} + \frac{\phi_{s,avg}}{R_{e_s}},
$$

Here R_{e_b}, R_{e_p} and R_{e_s} are the Reynolds numbers for bacteria, EPS and solvent, respectively, and $\phi b, p, s, avg$ are some chosen average volume fractions for bacteria, EPS and solvent, respectively. Then, the Gauge-Uzawa method is adopted in three steps below. We demonstrate the numerical scheme using the boundary conditions for the flow cell problem.

11

1. Prediction:

$$
\begin{cases}
\rho^{n+1}\frac{3\mathbf{u}^{n+1}-4\mathbf{v}^n+\mathbf{v}^{n-1}}{2\Delta t} + \rho^{n+1}\overline{\mathbf{v}}^{n+1}\cdot\nabla\overline{\mathbf{v}}^{n+1} + \frac{1}{2}(\nabla\cdot(\rho^{n+1}\overline{\mathbf{v}}^{n+1}))\overline{\mathbf{v}}^{n+1}, \\
\qquad +\frac{1}{R_{e_a}}\nabla s^n + \nabla p^n - \frac{1}{R_{e_a}}\nabla^2\mathbf{u}^{n+1} = \overline{\mathbf{R}}^{n+1} - \frac{1}{R_{e_a}}\nabla^2\overline{\mathbf{v}}^{n+1-\varepsilon}, \\
\qquad\qquad \mathbf{u}^{n+1}|_{y=0,L_y} = 0, \\
\qquad \mathbf{u}^{n+1}|_{x=0} = \mathbf{v}_0, \quad \mathbf{u}_x^{n+1}|_{x=L_x} = 0,
\end{cases}
\tag{22}
$$

2. Projection:

$$
\begin{cases}
-\nabla\cdot(\frac{1}{\rho^{n+1}}\nabla\psi^{n+1}) = & \nabla\cdot\mathbf{u}^{n+1}, \\
\frac{\partial\psi^{n+1}}{\partial n}|_{y=0,L_y} = & 0, \\
\frac{\partial\psi^{n+1}}{\partial n}|_{x=0,L_x} = & 0,
\end{cases}
\tag{23}
$$

3. Correction:

$$
\begin{cases}
\mathbf{v}^{n+1} = & \mathbf{u}^{n+1} + \frac{1}{\rho^{n+1}}\nabla\psi^{n+1}, \\
s^{n+1} = & s^n - \nabla\cdot\mathbf{u}^{n+1}, \\
p^{n+1} = & p^n - \frac{3\psi^{n+1}}{2\delta t} + \frac{1}{R_{e_a}}s^{n+1},
\end{cases}
\tag{24}
$$

where

$$
\overline{\mathbf{R}}^{n+1} = -\Gamma_1\nabla^2\overline{\phi}_n^{n+1}\nabla\overline{\phi}_n^{n+1} + \nabla\cdot(\overline{\phi}_b^{n+1}\overline{\tau}_b^{n+1} + \overline{\phi}_p^{n+1}\overline{\tau}_p^{n+1} + \overline{\phi}_s^{n+1}\overline{\tau}_s^{n+1}).
$$

Here $s^0 = 0$ and $v^1, s^1, \phi_b^1, \phi_p^1$ are computed by a first order scheme and $\varepsilon = 0.05$ is used.

After the momentum and continuity equations are solved, the calculated velocity data are used to update the phase field equations. Since $\phi_n = \phi_{bs} + \phi_{bp} + \phi_{bd} + \phi_p$, we obtain

$$
\nabla\mu_{bs} = \nabla\mu_{bp} = \nabla\mu_{bd} = \nabla\mu_p = -\Gamma_1\nabla(\nabla^2\phi_n) + \Gamma_2\left(\frac{1}{N}\frac{1}{\phi_n+\varepsilon} + \frac{1}{1-\phi_n} - 2\chi\right)\nabla\phi_n,
\tag{25}
$$

If we denote

$$
\mathcal{F}^{n+1}(\phi) = \left(\frac{1}{N}\frac{1}{\overline{\phi}_n^{n+1}+\varepsilon} + \frac{1}{1-\overline{\phi}_n^{n+1}} - 2\chi\right)\Gamma_2\nabla\phi - \Gamma_1\nabla\nabla^2\phi,
$$

the numerical schemes for the transport equations of the effective biomass components are given by

$$
\begin{aligned}
\frac{3\phi_{bs}^{n+1}-4\phi_{bs}^n+\phi_{bs}^{n-1}}{2\Delta t} + \nabla\cdot(\overline{\phi}_{bs}^{n+1}\mathbf{v}^{n+1}) &= \nabla\cdot\left(\Lambda\overline{\phi}_{bs}^{n+1}\mathcal{F}(\phi_{bs}^{n+1} + \overline{\phi_{bp}+\phi_{bd}+\phi_p}^{n+1})\right) + g_{bs}^{n+1}, \\
\frac{3\phi_{bp}^{n+1}-4\phi_{bp}^n+\phi_{bp}^{n-1}}{2\Delta t} + \nabla\cdot(\overline{\phi}_{bp}^{n+1}\mathbf{v}^{n+1}) &= \nabla\cdot\left(\Lambda\overline{\phi}_{bp}^{n+1}\mathcal{F}(\phi_{bp}^{n+1} + \overline{\phi_{bs}+\phi_{bd}+\phi_p}^{n+1})\right) + g_{bp}^{n+1}, \\
\frac{3\phi_{bd}^{n+1}-4\phi_{bd}^n+\phi_{bd}^{n-1}}{2\Delta t} + \nabla\cdot(\overline{\phi}_{bd}^{n+1}\mathbf{v}^{n+1}) &= \nabla\cdot\left(\Lambda\overline{\phi}_{bd}^{n+1}\mathcal{F}(\phi_{bd}^{n+1} + \overline{\phi_{bp}+\phi_{bd}+\phi_{bs}}^{n+1})\right) + g_{bd}^{n+1}, \\
\frac{3\phi_p^{n+1}-4\phi_p^n+\phi_p^{n-1}}{2\Delta t} + \nabla\cdot(\overline{\phi}_p^{n+1}\mathbf{v}^{n+1}) &= \nabla\cdot\left(\Lambda\overline{\phi}_p^{n+1}\mathcal{F}(\phi_p^{n+1} + \overline{\phi_{bp}+\phi_{bd}+\phi_{bs}}^{n+1})\right) + g_p^{n+1},
\end{aligned}
\tag{26}
$$

where

$$
\begin{aligned}
g_{bs1}^{n+1} &= \frac{C_2\overline{c}^{n+1}}{K_2+\overline{c}^{n+1}}(1-\frac{\overline{\phi}_{bs}^{n+1}}{\phi_{bs,\max}})\phi_{bs}^{n+1} - \overline{b}_{sp}^{n+1}\phi_{bs}^{n+1} + \overline{b}_{ps}^{n+1}\overline{\phi}_{bp}^{n+1} - (\frac{r_{bs}K_{sd}^2}{K_{sd}^2+(\overline{c}^{n+1})^2} + \frac{C_3\overline{d}^{n+1}}{K_3+\overline{d}^{n+1}})\phi_{bs}^{n+1}, \\
g_{bp1}^{n+1} &= \frac{C_4\overline{c}^{n+1}}{K_2+\overline{c}^{n+1}}(1-\frac{\overline{\phi}_{bp}^{n+1}}{\phi_{bp,\max}})\phi_{bp}^{n+1} - \overline{b}_{ps}^{n+1}\phi_{bp}^{n+1} + \overline{b}_{sp}^{n+1}\overline{\phi}_{bs}^{n+1}, \\
g_{bd}^{n+1} &= (r_{bs}\frac{K_{sd}^2}{K_{sd}^2+(\overline{c}^{n+1})^2} + \frac{C_3\overline{d}^{n+1}}{K_3+\overline{d}^{n+1}})\overline{\phi}_{bs}^{n+1} + r_{bp}\overline{\phi}_{bp}^{n+1} - r_{dp}\phi_{bd}^{n+1} - r_{bd}\phi_{bd}^{n+1}, \\
g_p^{n+1} &= \left(\frac{C_5\overline{c}^{n+1}}{K_5+\overline{c}^{n+1}}\overline{\phi}_{bs}^{n+1} + \frac{C_6\overline{c}^{n+1}}{K_6+\overline{c}^{n+1}}\overline{\phi}_{bp}^{n+1}\right)(1-\frac{\phi_p^{n+1}}{\phi_{p,\max}}) + r_{dp}\overline{\phi}_{bd}^{n+1} - r_p\phi_p^{n+1}.
\end{aligned}
\tag{27}
$$

Analogously, we use the updated data of the velocity and biomass to update the concentration of nutrient and antimicrobial agents, respectively. The transport equations for the nutrient and antimicrobial agents are given by

$$\frac{3\phi_s^{n+1}c^{n+1}-4\phi_s^n c^n+\phi_s^{n-1}c^{n-1}}{2\delta t} + \mathbf{v}^{n+1}\cdot\nabla(c^{n+1}\phi_s^{n+1}) = \nabla\cdot(D_c^{n+1}\phi_s^{n+1}\nabla c^{n+1}) + g_c^{n+1},$$
$$\frac{3\phi_s^{n+1}d^{n+1}-4\phi_s^n d^n+\phi_s^{n-1}d^{n-1}}{2\delta t} + \mathbf{v}^{n+1}\cdot\nabla(d^{n+1}\phi_s^{n+1}) = \nabla\cdot(D_e^{n+1}\phi_s^{n+1}\nabla d^{n+1}) + g_d^{n+1}, \tag{28}$$

where

$$g_c^{n+1} = -(\phi_{bs}^{n+1} + \mu_2\phi_{bp}^{n+1})\frac{C_7 c^{n+1}}{K_7+c^n},$$
$$g_d^{n+1} = -(C_8\phi_{bs}^{n+1} + C_9\phi_{bp}^{n+1} + C_{10}\phi_{bd}^{n+1} + C_{11}\phi_p^{n+1})\frac{d^{n+1}}{K_8+d^n}. \tag{29}$$

The schemes are presented as semi-discrete. The spatial discretization is carried out using the central difference. The boundary conditions are done using the biased finite difference at the boundary coupled with the central difference scheme for the equations. Grid refinement tests are carried out and nearly second order convergence in both time and space are achieved.

4 Numerical Results and Discussion

We note that there are many time and length scales in this hydrodynamic model. In this paper, a few selected regimes are studied which we think are important for the biofilm antimicrobial agent interaction. We consider two characteristic time scales for t_0: the growth time scale set at $t_0 = 10^3$ seconds, and, when simulating the biofilm treatment by antimicrobial agents with hydrodynamic flows involved, the antimicrobial agents and biofilm interaction time scale chosen as $t_0 = 10$ seconds. We remark that the time scale for biofilm treatment can vary from minutes to hours, or even days depending on the choice of the antimicrobial agents.

We summarize all the model parameters used in the current study in table (1) with their respective references therein. All the parameter values used in following simulations are chosen from table (1), unless noted otherwise.

4.1 Dynamics of reactive kinetics

Notice that the hydrodynamic model is consisted of 10 coupled partial differential equations and is quite complicated. Thus, it's advisable to study the bulk dynamics of the reactive kinetics first, before further investigating the hydrodynamics. Hence, by homogenizing the spatial effects, our model can effectively reduces to a system of coupled ordinary differential equations for a spatially homogeneous biofilm system:

$$\begin{cases} \frac{d\phi_{bs}}{dt} = \frac{C_2 c}{K_1+c}(1-\frac{\phi_{bs}}{\phi_{bs,\max}})\frac{\phi_{bs}^2}{\phi_{bs}+\phi_{\min}} - b_{sp}\phi_{bs} + b_{ps}\phi_{bp} - (\frac{r_{bs}K_{sd}^2}{K_{sd}^2+c} + \frac{C_3 d}{K_3+d})\phi_{bs}, \\[2mm] \frac{d\phi_{bp}}{dt} = \frac{C_4 c}{K_2+c}(1-\frac{\phi_{bp}}{\phi_{bp,\max}})\phi_{bp} + b_{sp}\phi_{bs} - b_{ps}\phi_{bp} - (r_{bp} + \frac{C_{12}d}{d+K_3})\phi_{bp}, \\[2mm] \frac{d\phi_{bd}}{dt} = (r_{bs}\frac{K_{sd}^2}{K_{sd}^2+c^2} + \frac{C_3 d}{K_3+d})\phi_{bs} + r_{bp}\phi_{bp} - r_{dp}\phi_{bd} - r_d\phi_d, \\[2mm] \frac{d\phi_p}{dt} = \left(\frac{C_5 c}{K_5+c}\phi_{bs} + \frac{C_6 c}{K_6+c}\phi_{bp}\right)(1-\frac{\phi_p}{\phi_{p,\max}}) + r_{dp}\phi_{bd} - r_p\phi_p, \\[2mm] \frac{dc}{dt} = -(\phi_{bs}+\mu_2\phi_{bp})\frac{C_7 c}{K_7+c} + C_{13}(c0 - c), \\[2mm] \frac{dd}{dt} = -(C_8\phi_{bs}+C_9\phi_{bp}+C_{10}\phi_{bd}+C_{11}\phi_p)\frac{d}{K_8+d}, \end{cases} \tag{30}$$

13

where

$$b_{sp} = \left(b_{sp1}\frac{k_{spc}^{n_c}}{k_{spc}^{n_c}+c^{n_c}} + b_{sp2}\frac{d^{n_d}}{k_{spd}^{n_d}+d^{n_d}}\right)\left(1 - \frac{\phi_{bp}}{\phi_{bp,\max}}\right),$$
$$b_{ps} = b_{ps,\max}\frac{c^{m_c}}{k_{psc}^{m_c}+c^{m_c}}\frac{k_{psd}^{m_d}}{k_{psd}^{m_d}+d^{m_d}}. \tag{31}$$

We note that, in our spatial-temporal hydrodynamic model, nutrient is transported into the biofilm by diffusion. The last term in nutrient equation above is modified to account for this feature, where c_0 is the nutrient concentration in the surroundings. The reactive dynamics of the system of equations is studied using Matlab ODE solvers.

When the biofilm grows without antimicrobial treatment, all bacteria reproduce provided that the nutrient supply is sufficient. Since the susceptible cells are more metabolically active, their population grows exponentially until it reaches the carrying capacity of the environment. At the same time, there exist dynamics of conversion between the susceptible and the persister cells. Here, we simulate the spatially homogeneous biofilm development by varying the maximum conversion rates between the susceptible and the perisister cells, i.e., b_{sp1} and $b_{ps,\max}$, respectively. The result is shown in figure 1 and figure 2. Note that b_{sp2} doesn't have an effect in this case since $d = 0$. As shown in Figure 1, with a higher conversion rate b_{sp1}, the persister has a higher volume fraction in steady state. A higher volume fraction of the persister is also observed by lowering conversion rate b_{ps} in Figure 2. The conversion rates mainly affect the susceptible and persister populations and have little impact on the other components in the biofilm as expected. This study shows that the growth dynamics of the persister is highly dependent on the conversion rates between the susceptible and the persister.

The dynamics of biofilm being treated by antimicrobial agents are summarized in Figure 3 with respect to both constant dosing and periodic dosing strategies. If we keep dosing constantly, see Figure 3, the biofilm growth could be controlled/contained but not be eliminated, as the susceptible cells could be eradicated but the persisters are affected only slightly. However, if we dose the sample periodically, that's one dosage for a while and ceases the dosage for a period and then repeat the process again, the bacteria in the biofilm can eventually be eradicated completely shown in Figure 3. These predictions agree qualitatively with the literature [8] in that the periodic dosing strategy is viewed as an advisable way to eliminate the biofilm.

One important issue pertinent to the conversion of susceptible and persister cells is how these two bacterial phenotypes convert and how fast they convert to one another. While we can't find any timely experimental evidence to guide us in this study apparently, we resort to a systematic study using our proposed model. Due to the lack of refined studies in this direction, most of the literature, such as [18], regard b_{sp} and b_{ps} as constants. Besides, Cogan [8] used nonconstant and nonlinear conversion rate functions:

$$b_{sp} = b_{sp1}\frac{c}{c+k_{sp}}, \quad b_{ps} = b_{ps,\max}\left(1 - \frac{1}{1+e^{-\frac{d-d_0}{\varepsilon}}}\right), \tag{32}$$

where b_{sp1} and $b_{ps,\max}$ are the maximum conversion rates and d_0 is the threshold for antimicrobial agents, ε is a small parameter. However, we note that these proposals are still not quite satisfactory.

To benchmark the choices of the conversion rates adopted in our model, we conduct several additional numerical simulations to compare the constant conversion rates between the Cogan's proposal in [8] and our proposal in equation (20). The results are shown in Figure 4.

In Figure 4 (a), for a well-grown biofilm with depleted nutrient in the end, both the susceptible and the persister cells gradually diminish in the case of constant conversion rates or Cogan's proposal for the conversion rates. These are in direct conflict with the experimental observations where persisters are in a dormant status [28] and could survival in a nutrient depleted environment [31] [5], as least for a

14

quite long period of time. In comparison, our proposed rates agree qualitatively well with the survival persisters in the experiments in which the persister decays slightly.

Figure 4(b) depicts a scenario in which the biofilm is being treated with antimicrobial agents. Note that we only plot the data with the constant conversion rates and our proposal, as Cogan's conversion rates predict almost the same as ours for the susceptible in this case. For the constant conversion rates, all bacteria are eventually killed. However, this is not the case in the reality since many experiments reported that a small portion of bacteria would survive the antimicrobial treatment, no matter how long or how strong the antimicrobial doses are kept [28], which is exactly what are observed using the conversion rates in equation (20) proposed in this paper. So, our proposed conversion rates can handle both persister survival due to nutrient depletion and antimicrobial treatment.

4.2 Heterogeneous biofilm development without the antimicrobial treatment

Our main interest in this paper is the mechanism of biofilm persistence to antimicrobial agents coupled with heterogeneous biofilm colonies. Before digging into the issue, we would like to benchmark the model for biofilm formation without antimicrobial treatment as well as demonstrate the capability of our proposed model for capturing details of biofilm formation in space and time. In particular, how EPS production can impact on the growth of spatial-temporal heterogeneous structures in biofilms and cell starvation due to nutrient depletion influences biofilm structures during biofilm formation will be studied in detail.

4.2.1 Heterogeneous biofilm structures regulated by EPS production

It's commonly perceived that EPS plays an essential role in the formation and maintenance of the structural stability of biofilms [29] and that EPS production rate could affect the biofilm structure dramatically. In order to study the role of EPS production in the process of biofilm formation, 3-D numerical simulations are conducted. Our numerical study agrees qualitatively with the spatial variation in EPS production [9], which leads to gradients in osmotic pressure and contributes to pattern formation of mushroom or tower shaped.

Figure 5 depicts two numerical simulations with respect to varying EPS growth rates. It reveals that the role of EPS production is to expand the biofilm colony such that the higher the EPS production rate is, the thicker the biofilm colony can grow. The biofilm growth without EPS production yields a slower growth of the biofilm colony.

These numerical evidence validates the notion about the role of EPS production in biofilm formation [37]. Though higher EPS production would consume more nutrient, while in the meantime limits the supply of nutrient to bacteria. In the case where the nutrient supply is sufficient by diffusive transportation, bacteria would not be affected negatively. However, higher EPS production could help to expand the biofilm colonies, as a result, bacteria could access more nutrient with larger surface contact with the solvent, which in turn help bacteria to grow.

4.2.2 Effect of nutrient depletion on heterogeneous biofilm structures

In addition to EPS production, other factors may affect the structure of biofilm colonies during their development as well, one of which is the bacterial death factor. There are several causes that could lead to bacterial death. These include programmed cell death [27], metabolic toxins [30], competition of different species [34] and starvation [7]. Starvation is the phenomenon about bacterial death due to nutrient depletion, i.e., the bacterial cells are starved to death while the nutrient nearby is exhausted. At the presence of cell death, it has been observed that biofilms could form a hollow structure (void or channel) due to the decomposition of the dead bacteria into solvent and EPS in the biofilm [24].

15

We carry out a numerical experiment coupled with the modified decay rate shown in Figure 6, where void structure is observed, as dead bacteria and parts of EPS are dissolved into the solvent. Since the nutrient is supplied on the top, the level of nutrient is low at the bottom part of the domain, as shown in figure 7(c). Initially, when nutrient supply is still sufficient, the susceptible bacteria grows homogeneously. Later, bacteria at the bottom have less access to nutrient. As it could be observed, this results in the competition for nutrient leading to partial death of the susceptible bacteria. Thus, the live susceptible bacteria is mainly distributed in the upper part of biomass, where there are more access to nutrient. Besides, the susceptible is more metabolically active, as could be seen that the nutrient consumption rate is much higher at the biomass surface in figure 7(b), where it is consumed by susceptible bacteria. In the meanwhile, the persister mainly distributed in the lower part, where there is little access to nutrient, since it is in a dormant state [28], saying metabolic inactive. The biomass flux is mainly at the top surface of biofilm colony, which shows that nutrient competition drives the biofilm to expand. Besides, the averaged velocity is much stronger, where there are more volume of biomass.

In figure 6(i), we observe the mushroom shape of the overall-biomass growth morphology. By adding the feature of death from starvation and competition for nutrient, our model could capture heterogenous biofilm structure qualitatively. We note that, besides nutrient competition, hydrodynamic stress would also affect the structure of biofilm, as well as the distributions of its components. In this simulation, biofilm is grown in a quiescent environment, thus hydrodynamics stress is not as effective as nutrient competition in contributing heterogeneous biofilm formation.

4.3 Biofilm Development and the impact of antimicrobial agents

The concept that biofilm contains both persisters and susceptible bacterial cells has been around for a while. Lewis [28] has hypothesized that persisters are the main reason for persistent mechanism of bacteria cells to antimicrobial agents in biofilms. In addition to the existence of persisters, some argues that EPS acts as a viscous gel that could prevent antimicrobial agents from penetrating deep into biofilms to access the internal bacterial cell; while others propose that EPS could dilute the concentration of antimicrobial agents by reacting with it [42]. Besides, the dead bacteria may also act as a shield for the biofilm.

In the following subsections, we study the mechanism that makes bacteria living within a biofilm more tolerable than planktonic bacteria with respect to antimicrobial treatment. Later in this section, the effect of the conversion rate between susceptible and persister bacteria for heterogeneous biofilms will be discussed. Specifically, we conduct 3-D numerical simulations using our model to reveal the antimicrobial treatment of heterogeneous biofilms and attest the hypothesis of the existence of persisters and slow penetration of antimicrobial agents due to EPS, as well as dead bacteria. Then, we show that the periodic dosing strategy is indeed a better way compared with constant dosing in eradicating the bacteria in heterogeneous biofilms. For convenience, the initial biomass distribution for later simulations are summarized in figure 8. We note that higher EPS ratio in grown biofilm is usually observed in hydrodynamic environment. And we set the volume fraction of persister bacteria to be zero in second case, in order to depict in details the converting process from the susceptible to persister during antimicrobial treatment in later simulations.

4.3.1 Antimicrobial treatment and biofilm control

To develop a proper strategy for biofilm control, a clear understanding of the disinfecting process in heterogeneous biofilms is necessary. With the 3-D numerical tool, we investigate the disinfecting process in a long fluid channel as well as a short flow cell, during which various dosing positions will be examined.

As shown in Figure 9, we mimic the situation where the biofilm develops in a tank with quiescent solvent and antimicrobial agents supplied in a well-mixed form with the pure solvent from the top boundary. In reality, this scenario agrees with the case of spraying antimicrobial solution on the biofilm surface. Given a well-grown biofilm, once we start dosing antimicrobial agents, the susceptible cells will be killed drastically. However, the volume fraction of the persisters retains at a stable level, as well as EPS. In other words, this dosing method fails to eradicate the grown biofilm colony completely, which is always the case in reality.

The second numerical experiment mimics the situation of disinfection in a flow-cell, where the antimicrobial agents are well-mixed with the solvent and flown in from the inlet boundary. In reality, this approximates the disinfection of biofilms, growing in a river bed or in a water pipe. The simulation results are shown in Figure 10. Unlike the case alluded to earlier, the distribution of dead bacteria is heterogeneous, namely, more susceptible bacteria are killed facing the inlet boundary than facing the downstream due to the heterogeneous distribution of antimicrobial agents. In the meanwhile, some susceptible bacteria are converted into persister bacteria, as the existence of antimicrobial agents triggered this conversion. In order to depict more details, 2D slices at $z = 0.5$ are shown in figure 11. As could be observed, antimicrobial agents are distributed heterogeneously, as well as its consumption rates. Due to the limitation of antimicrobial diffusive rate into biofilm, they are not consumed totally at the inlet boundary, but convected through the domain. Effective hydrodynamic pressure is high at the inlet boundary and low in the channels of biofilm colonies. We note that there is biomass flux towards the outlet boundary, as shown in figure 11(f). However, the biofilm is in a laminar flow, thus its the disinfection process that dominate the dynamics. Similar with the previous case, persisters can survive this treatment, in other words, this dosing method also fails to eradicate the biofilm colony satisfactorily.

We note that, to the best of our knowledge, most mathematical models available treating antimicrobial agents as well-mixed with solvent and thereby describe the antimicrobial agents using a spatially homogeneous differential equation (ODE). In real applications however, we must take into account the heterogeneous distribution of antimicrobial agents and biofilm structures. Therefore, we consider an injection of antimicrobial agents into the solvent by a needle. After the injection, the antimicrobial distribution within the biofilm ambient fluid ensemble is dominated by convection and diffusion of antimicrobial agents through various media. As far as we know, it is the first mathematical biofilm model and simulation in the literature to show this full 3D view of disinfection process by antimicrobial injection. Figure 12 depicts the simulation details. During the process, persisters are converted from susceptible bacteria and the killing of bacteria is asymmetric and heterogeneous in space and time. The concentration of the dead bacteria close to the source of the antimicrobial agents is apparently much higher than that on the other side of the biofilm colony. The persister cell concentration doesn't drop at the dosing position, in other words, persisters survive this treatment as well.

Despite that constant dosing shown in the simulations can not eradicate the bacteria in the biofilm colony completely, our model suggests that targeted disinfection, i.e., disinfection by injection to the specific position, is more efficient and environmental-friendly since it requires less amount of antimicrobial agents to achieve the same effect, especially for biofilms grown in an aqueous system, where the flow velocity is not too small to be ignored. With the development of nanotechnology, targeted delivery of antimicrobial agents directly to the biofilm is becoming an reality and is shown to be more efficient. Moreover, since EPS could prevent antimicrobial agents from diffusing away from the biofilm, the local antimicrobial concentration could be maintained for longer period of time.

We note that the diffusion rate of antimicrobial agents is partially responsible for the heterogeneous distribution of dead bacteria. If the diffusion rate of antimicrobial agents is high, the distribution of dead bacteria would be homogeneous with respect to biofilm colonies. But If the diffusion rate is small, in other words, the transport in the biofilm-solvent system is convection dominated, the density of dead bacteria would be highly heterogeneous with higher concentration near the dosing position.

17

Observed from the disinfection process above, every constant dosing case fails to eradicate all the bacteria in one long dose. Therefore, a straightforward question is: what happened to the biofilm after the cessation of an antimicrobial dosing? One simulation result is shown in Figure 13 with the initial biofilm colony from the experiment in Figure 9. After dosing stops and the concentration of antimicrobial agents drops below the threshold, persisters become active from dormant status and convert back into susceptible cells for proliferation. This leads to the relapse of biofilm growth after certain period of time. The newly grown biofilm is morphologically similar with previous colony, as could be observed. Besides, we also absolve that the susceptible bacteria mainly distributed at the surface of biomass, where they have more access to nutrient. But, the persister bacteria is less metabolical active [28], staying at the bottom of the biomass, where there is less nutrient.

4.3.2   Slow penetration effects due to EPS and dead bacteria

It's commonly known that bacteria living in a biofilm are more persistent to antimicrobial treatment than planktonic bacteria. Besides the existence of persister cells, reason for this phenomenon is that EPS can acts as a shield for trapped bacteria and thereby could retard or even prevent the antimicrobial agents from penetrating deeper into the biofilm colony. Another potential shield is that some dead bacteria would gather on some internal surface of the biofilm, which also makes it harder for the antimicrobial agents to diffuse into the biofilm .

We investigate the phenomenon of antimicrobial penetration using our model in 3-D simulations for varying diffusion rate of antimicrobial agents proposed in equations (5),(6),(7). Initially we begin with a well-grown biofilm in the center of the domain, the simulation results for the three cases with distinct diffusion coefficients are shown in Figure 14. Slow penetration effects due to EPS, as well as dead bacteria, are observed during the disinfection process.

The total volume fraction of each component after antimicrobial treatment is shown in Figure 15. The difference is the varying decay rate of susceptible bacteria due to slow penetrating effect induced by EPS and dead bacteria. Details of the susceptible decaying rate is shown in Figure 15(A). Due to the slower penetration of antimicrobial agents at the presence of EPS and bacteria, the survival curve drops slower than the controlled set, i.e. constant diffusion rate proposed in equation (5), since more susceptible bacteria survive and they could mutate into persisters. This gives a convincing explanation that EPS acts as a shield for the bacteria [16].

However, apparently from (E) in Figure 15, each case fails to eradicate the bacteria in the biofilm, as a small portion of persisters is hardly affected by antimicrobial agents shown in Figure 15(C). On the other hand, our numerical results demonstrate that the slow penetration caused by EPS and bacteria distribution does slow down the antimicrobial treatment of the biofilm. However, it only shows as a factor for retarding the treatment of biofilm, but not the essential component for antimicrobial persistence of biofilm.

4.3.3   Dosing strategy

As reported in [28] experimentally as well as predicted by our biofilm model, antimicrobial agents fails to eradicate all the bacteria in one long dose. After the dosing is stopped, the bacterial growth can relapse. Thus, searching for an optimal dosing strategy is necessary.

When dosing strategies are considered, basically, there are two ways to carry it out. One is to give high concentrated doses of antimicrobial agents in short time period and the other is to give low concentration doses of antimicrobial agents continuously at a long time period. The question here to discuss is which way is better. Although several research articles have discussed this issue for homogeneous biofilms [39], [19], [20] and [8], it is worthy of exploring the solution in a heterogeneous biofilm. In

18

addition, the poorly understood mechanism of biofilm resistance to antimicrobial agents, more practical issues arise recently, such as the cost of antimicrobial agents and the requirement of environmentally friendly antimicrobial agents [19], which demands less usage of antimicrobial agents to control the biofilm.

As previously studied, constant dosing could control the bacteria to within a low level, but it can leave a small portion of them alive, most of which are persisters. Since the conversion rate of persisters to susceptible cells with existing antimicrobial agents is relatively small, instead of being killed by changing into susceptible bacteria, persisters could keep its number stable for a quite long period of time. Thus, after the susceptible cells are eradicated, a short period of ceased dosing is in favor for facilitating the persister conversion into susceptible cells, which can then be killed easily by the subsequent dosages. In Figure 16, for a given, well-grown biofilm, we dose antimicrobial agents for 10 units of time, where $t_0 = 1000$ seconds and then cease dosing for 20 units of time, and then repeat this process. Following this strategy, both the susceptible and the persister cells can be killed eventually.

With this hydrodynamic model, we confirm the hypothesis that periodic dosing strategies give higher disinfection rate and could eradicate all the bacteria or to reduce its concentration to under a prescribed, lower level within a short period of time provided that the dosing period and dosing strength is well controlled.

5   Conclusion

In this paper, we extend our previous phase field models for biofilms [47], [48] to multiphasic biofilms by taking into account multiple types of bacteria and the effect of antimicrobial agents. Then, a series of three dimensional numerical simulations are carried out to investigate biofilm development both with and without antimicrobial treatment.

For naturally growing biofilms without antimicrobial treatment, our model verifies the hypothesis that the production of extra polymeric substances promotes the spreading of biofilms by generating osmotic pressure [37]. In addition, the void structure of the biofilm morphology due to nutrient depletion can also be captured, which qualitatively agrees with the experiment observation [15].

For the antimicrobial treated biofilms, both antimicrobial treatment in an infinite-long channel and a finite-long tube, along with varying dosing positions and strategies are investigated. As suggested from the numerical simulations, the mechanism of conversion between the susceptible bacteria and persisters is essential for the growth dynamics of persisters.

Besides persisters, EPS and dead bacteria can form obstacles to hinder the diffusion of antimicrobial agents, which, in turn, protects biofilm from being disinfected quickly. As a result, it provides more time for susceptible bacteria to transform into persisters. The mechanisms of retarding the antimicrobial diffusion by EPS and dead bacteria make biofilms even harder to be disinfected.

It is difficult to eradicate biofilms completely by conventional means. Thus, proper strategies are in need for biofilm control. As is observed from the numerical simulations, dosing by injection is much more efficient, as well as environment-friendly, than using a nebulizer, which delivers the antimicrobial agent to the surface of the biomass-solvent mixture. Especially, antimicrobial agent-carrying nano spheres, which could be imbedded within the biofilm, would be much more efficient, as EPS would prevent the antimicrobial agents from diffusing away from the biofilm. Besides the dosing position, dosing strategies are also vital for effective disinfection. Our numerical simulations, consistent with experiments reported in literature, confirm that the periodic dosing would make a better biofilm control than dosing for one time or continuous dosing [19].

In general, the three dimensional heterogeneous biofilm model is capable of capturing details of biofilm development and morphological changes during antimicrobial treatment. It provides an in-silico

tool for analysing the mechanism of biofilm persistence to antimicrobial agents and deriving potentially optimal dosing strategies for biofilm control or disease treatment.

Acknowlegement

References

[1] Erik Alpkvist, Cristian Picioreanu, Mark C. M. van Loosdrecht, and Anders Heyden. Three-dimensional biofilm model with individual cells and continuum eps matrix. *Biotechnology and Bioengineering*, 94(5):961–979, August 2006.

[2] Stephanie M. Amato, Mehmet A. Orman, and Mark P. Brynildsen. Metabolic control of persister formation in escherichia coli. *Molecular Cell*, 50(4):475–487, May 2013.

[3] Nathalie Q. Balaban, Jack Merrin, Remy Chait, Lukasz Kowalik, and Stanilas Leibler. Bacterial persistence as a phenotypic switch. *Science*, 305(5690):1622–1625, August 2004.

[4] Kenneth W. Bayles. The biological role of death and lysis in biofilm development. *Nature Reviews Microbiology*, 5(9):721–726, September 2007.

[5] Steve P. Bernier, David Lebeaux, Alicia S. DeFrancesco, and etc. Starvation together with the sos response mediates high biofilm-specific tolerance to the fluoroquinolone ofloxacin. *PLoS Genetics*, 9(1), 2013.

[6] Giorgia Borriello, Lee Richards, Garth D. Enrlich, and Philip S. Stewart. Arginine or nitrate enhances antibiotic susceptibility of pseudomonas aeruginosa in biofilms. *Antimicrobial Agents and Chemotherapy*, 50(1):382–384, January 2006.

[7] Jason D. Chambless, Stephen M. Hunt, and Philip S. Stewart. A three-dimensional computer model of four hypothetical mechanisms protecting biofilms from antimicrobials. *Applied and Environmental Microbiology*, 72(3):2005–2013, March 2006.

[8] N. G. Cogan, Brown J, Darres K, and Petty K. Optimal control strategies for disinfection of bacterial populations with persister and susceptible dynamics. *Antimicrobial Agents and Chemotherapy*, 56(9):4816–4826, September 2012.

[9] N. G. Cogan and James P. Keener. The role of the biofilm matrix in structural development. *Mathematical Medicine and Biology*, 21(2):147–166, 2004.

[10] N. G. Cogan, Barbara Szomolay, and Martin Dindos. Effects of periodic disinfection on persisters in a one-dimensional biofilm model. *Bulletin of Mathematical Biology*, 75:94–123, 2013.

[11] N.G. Cogan. Effects of persister formation on bacterial response to dosing. *Journal of Theoretical Biology*, 238:694–703, February 2006.

[12] David Davies. Understanding biofilm resistance to antibacterial agents. *Nature Reviews Drug Discovery*, 2:114–122, February 2003.

[13] L. Demaret, J. H. Eberl, M. A. Efendiev, and R. Lasser. Analysis and simulation of a meso-scale model of diffusive resistance of bacterial biofilms to penetration of antibiotics. *Advances in Mathematicsl Sciences and Applications*, 18:269–304, 2008.

[14] Tobias Dorr, Marin Vulic, and Kim Lewis. Ciprofloxacin causes persister formation by inducing the tisb toxin in escherichia coli. *PLoS Biology*, 8(2), 2010.

[15] Magnus G. Fagerlind, Jeremy S. Webb, and etc. Dynamic modelling of cell death during biofilm development. *Journal of Theoretical Biology*, 295:23–26, 2012.

[16] Hans-Curt Flemming, Thomas R. Neu, and Daniel J. Wozniak. The eps matrix: The "house of biofilm cells". *Journal of Bacteriology*, 189(22):7945–7947, November 2007.

[17] Hans-Curt Flemming and Jost Wingender. The biofilm matrix. *Nature Reviews Microbiology*, 8:623–633, September 2010.

[18] Orit Gefen and Nathalie Q. Balaban. The importance of being persistent: heterogeneity of bacterial populations under antibiotic stress. *FEMS Microbiology Reviews*, 33(4):704–717, 2009.

[19] D. M. Grant and T. R. Bott. Biocide dosing strategies for biofilm control. *Heat Transfer Enginnering*, 26(1):44–50, 2005.

[20] K.J. Grobe, J. Zahller, and P.S. Stewart. Role of dose concentration in biocide efficacy against pseudomonas aeruginosa biofilms. *Journal of Industrial Microbiology and Biotechnology*, 29:10–15, 2002.

[21] J.L. Guermond, P. Minev, and Jie Shen. An overview of projection methods for incompressible flows. *Computer Methods in Applied Mechanics and Engineering*, 195:6011–6045, 2006.

[22] R. Hinson and W. Kocher. Model for effective diffusivities in aerobic biofilms. *Journal of Environmental Engineering*, 122(11):1023–1030, 1996.

[23] S. M. Hunt, M. A. Hamilton, and P.S. Stewart. A 3d model of antimicrobial action on biofilms. *Water Science and Technology*, 52(7):143–148, 2005.

[24] Stephen M. Hunt, Erin M. Werner, Baochuan Huang, Martin A. Hamilton, and Philip S. Stewart. Hypothesis for the role of nutrient starvation in biofilm detachment. *Applied and Environmental Microbiology*, 70(12):7418–7425, December 2004.

[25] Isaac Klapper and Jack Dockery. Mathematical description of microbial biofilms. *SIAM Review*, 52(2):221–265, may 2010.

[26] Patrick De Leenheer and N. G. Cogan. Failure of antibiotic treatment in microbial populations. *Journal of Mathematical Biology*, 59(4):563–579, 2009.

[27] Kim Lewis. Persister cells dormancy and infectious disease. *Nature Reviews Microbiology*, 5:48–56, 2007.

[28] Kim Lewis. Persister cells. *Annual Review of Microbiology*, 64(1):357–372, 2010.

[29] Yong-Qiang Liu, Yu Liu, and Joo-Hwa Tay. The effects of extracellular polymeric substances on the formation and stability of biogranules. *Applied Microbiology and Biotechnology*, 65:143–148, 2004.

[30] Van Melderen, Laurence, Saavedra De Bast, and Manuel. Bacterial toxin-antitoxin systems: More than selfish entities? *PLoS Genetics*, 5(3):e1000437, 03 2009.

[31] Dao Nguyen, Amrutat Joshi-Datar, and etc. Active starvation responses mediate antibiotic tolerance in biofilms and nutrient-limited bacteria. *Science*, 334:982–986, 2011.

[32] Cristian Picioreanu, Mark C. M. van Loosdrecht, and Joseph J. Heijnen. Mathematical modeling of biofilm structure with a hybrid differential discrete cellular automaton approach. *Biotechnology and Bioengineering*, 58(1):101–116, April 1998.

[33] Keith Poole. Bacterial stress responses as determinants of antimicrobial resistance. *Journal of Antimicrobial Chemotherapy*, 20(5):227–234, May 2012.

[34] Olaya Rendueles and Jean-Marc Ghigo. Multi-species biofilms: how to avoid unfriendly neighbors. *FEMS Microbiology Reviews*, 36(5):972–989, 2012.

[35] Mark E. Roberts and Philip S. Stewart. Modeling protection from antimicrobial agents in biofilms through the formation of persister cells. *Microbiology*, 151:75–80, 2005.

[36] Jose A. Sanclement, Paul Webster, John Thomas, and Hassan H. Ramadan. Bacterial biofilms in surgical specimens of patients with crhonic rhinosinusitis. *Laryngoscope*, 115(4):578–582, April 2005.

[37] Agnese Seminara, Thomas E. Angelini, James N. Wilking, Hera Vlamakis, Senan Ebrahim, Roberto Kolter, David A. Weitz, and Michael P. Brenner. Osmotic spreading of bacillus subtilis biofilms driven by an extracellular matrix. *PNAS*, 2012.

[38] Zhiya Sheng and Yang Liu. Effects of silver nanoparticles on wastewater biofilms. *Water Research*, 45:6039–6050, 2011.

[39] Manuel Simões, Lúcia C. Simões, and Maria J. Vieira. A review of current and emergent biofilm control strategies. *LWT - Food Science and Technology*, 43(4):573 – 583, 2010.

[40] P S Stewart. Theoretical aspects of antibiotic diffusion into microbial biofilms. *Antimicrobial Agents and Chemotherapy*, 40(11):2517–22, 1996.

[41] Philip S. Stewart. Diffusion in biofilms. *Journal of Bacteriology*, 185(5):1485–1491, Mar 2003.

[42] Ian W. Sutherland. Biofilm exopolysaccharides: a strong and sticky framework. *Microbiology*, 147(1):3–9, 2001.

[43] Barbara Szomolay, Isaac Klapper, and Martin Dindos. Analysis of adaptive response to dosing protocols for biofilm control. *SIAM Journal of Applied Mathematics*, 70(8):3175–3202, 2010.

[44] Qi Wang and Tianyu Zhang. Review of mathematical models for biofilms. *Solid State Communications*, 150(21):1009–1022, June 2010.

[45] Qi Wang and Tianyu Zhang. Kinetic theories for biofilms. *Discrete and Continuous Dynamical Systems Series B*, 17(3):1027–1059, May 2012.

[46] James N. Wilking, Thomas E. Angelini, Agnese Seminara, Michael P. Brenner, and David A. Weitz. Biofilms as complex fluids. *MRS Bulletin*, 36(5):385–391, May 2011.

[47] Tianyu Zhang, Nick G. Cogan, and Qi Wang. Phase-field models for biofilms i. theory and simulations. *SIAM Journal of Applied Mathematics*, 69:641–669, 2008.

[48] Tianyu Zhang, Nick G. Cogan, and Qi Wang. Phase-field models for biofilms ii. 2-d numerical simulations of biofilm-flow interaction. *Communication in Computational Physics*, 4(1):72–101, July 2008.

Symbol	Description	value	Unit	Source
T	absolute temperature	303	Kelvin	[47]
k_B	Boltzmann constant	1.38065×10^{-23}	$m^2 kg s^{-2}$	[47]
ρ_n	biomass density	1×10^3	$kg\ m^{-3}$	[47]
ρ_s	water density	1×10^3	$kg\ m^{-3}$	[47]
h	characteristic length scale	1×10^{-3}	m	[32]
t_0	characteristic time scale	10 or 1000	s	[47]
L_x, L_y, L_z	size of computational domain	$1 - 2 \times 10^{-3}$	m	[47]
η_b	dynamic viscosity of bacteria	2.7×10^2	$kg\ m^{-1} s^{-1}$	[25]
η_p	dynamic viscosity of EPS	2.7×10^2	$kg\ m^{-1} s^{-1}$	[25]
η_s	dynamic viscosity of solvent	1.002×10^{-3}	$kg\ m^{-1} s^{-1}$	[25]
c_0	characteristic oxygen concentration	8.24×10^{-3}	$kg\ m^{-3}$	[32]
d_0	characteristic antimicrobial concentration	8.24×10^{-3}	$kg\ m^{-3}$	
γ_1	distortional energy coefficient	8×10^6	m^{-1}	
γ_2	mixing free energy coefficient	3×10^{17}	m^{-3}	
χ	Flory-Huggins parameter	0.55		[47]
λ	mobility parameter	1×10^{-9}	$kg^{-1} m^3 s$	
N	generalized polymerization parameter	1×10^3		[47]
D_c	oxygen diffusion coefficient	2.3×10^{-9}	$m^{-2} s^{-1}$	[41] , [32]
D_d	antimicrobial diffusion coefficient	2.3×10^{-8}	$m^{-2} s^{-1}$	[41]
D_{pr}	Hinson model parameter	0.02		[22]
$\phi_{bs,\max}$	carrying capacity for susceptible bacteria	0.2		
$\phi_{bp,\max}$	carrying capacity for persister	0.02		
$\phi_{p,\max}$	carrying capacity for EPS	0.2		
C_2	susceptible bacteria growth rate	4×10^{-4}	s^{-1}	
C_3	susceptible bacteria decaying rate	4×10^{-2}	s^{-1}	
C_4	persist bacteria growth rate	4×10^{-7}	s^{-1}	
C_{12}	persister bacteria decay rate	4×10^{-5}	s^{-1}	
$r_{bs,\max}$	flush-out rate for susceptible	4×10^{-7}	s^{-1}	
r_{bp}	flush-out rate for persister	1×10^{-7}	s^{-1}	
r_{bd}	flush-out rate for dead bacteria	1.0×10^{-7}	s^{-1}	
b_{sp1}	transfer rate	1×10^{-5}	s^{-1}	
b_{sp2}	transfer rate	1×10^{-3}	s^{-1}	
k_{spd}, k_{spc}	Monond constant for b_{sp}	3.5×10^{-4}	$kg\ m^{-3}$	
$b_{ps,\max}$	transfer rate from ϕ_{bs} to ϕ_{bp}	4×10^{-5}	s^{-1}	
k_{psc}, k_{psd}	Monod constant for b_{ps}	3.5×10^{-4}	$kg\ m^{-3}$	
m_c, m_d, n_c, n_d, n	Hill parameter	2		
C_5	EPS growth rate due to susceptible	4×10^{-4}	s^{-1}	
C_6	EPS growth rate due to persisters	4×10^{-6}	s^{-1}	
r_p	flush-out rate for EPS	4×10^{-7}	s^{-1}	
r_{dp}	converting rate from death bacteria to EPS	4×10^{-7}	s^{-1}	
C_7	nutrient consumption rate	4×10^{-2}	$kg\ m^{-3}\ s^{-1}$	
μ_2	nutrient consumption rate(ϕ_{bs} v.s. ϕ_{bp})	0.1		
k_{cd}	Monond constant for r_{bd}	3.5×10^{-4}		
C_8, C_9	antimicrobial agents consumption rate	4×10^{-2}	$kg\ m^{-3}\ s^{-1}$	
C_{10}, C_{11}	antimicrobial agents consumption rate	4×10^{-4}	$kg\ m^{-3}\ s^{-1}$	
K_2, K_3, K_5, K_6, K_8	monod constant for EPS growth	3.5×10^{-4}	$kg\ m^{-3}$	[32]

Table 1: The table for parameter values. All parameters with resources are marked. The others are fitted from our previous work and experiment results.
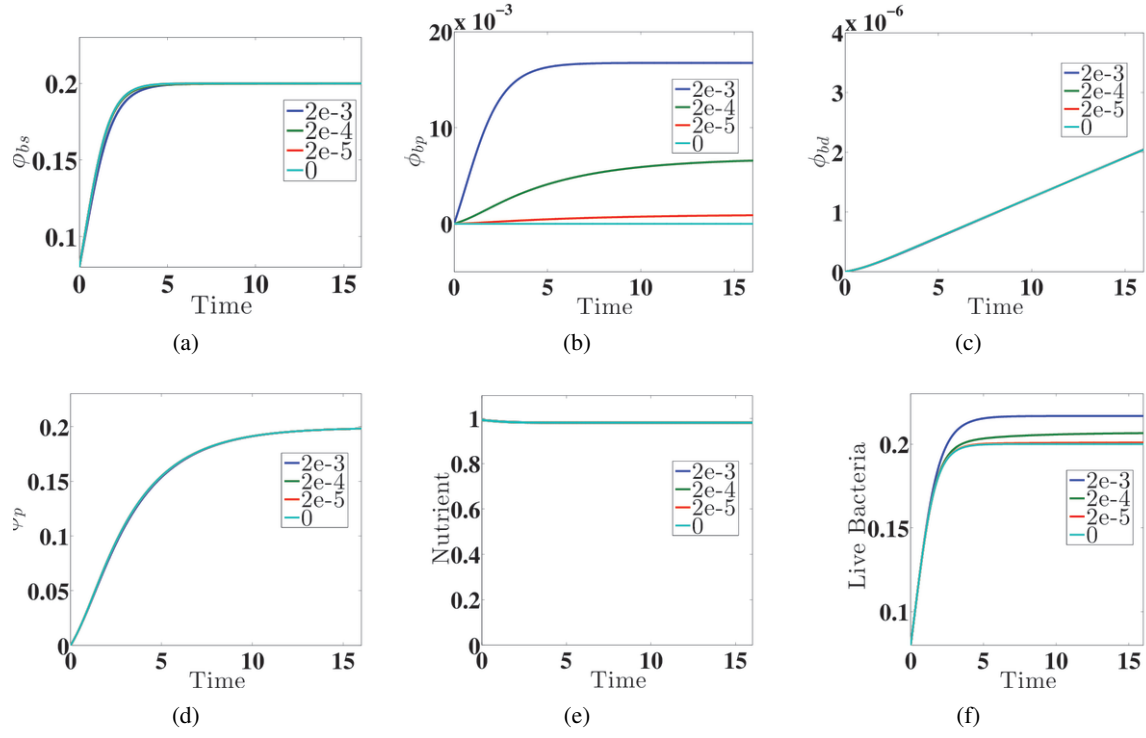
Figure 1: Growth dynamics of spatially homogeneous biofilms. This figure shows biofilm growth dynamics with respect to four selected conversion rate b_{sp1}: $0, 2 \times 10^{-5}, 2 \times 10^{-4}, 2 \times 10^{-3}$. The volume fractions of the susceptible, persister, dead bacteria, EPS and the concentration of nutrient and total volume fraction of live bacteria with time are shown in (a)-(f) respectively.
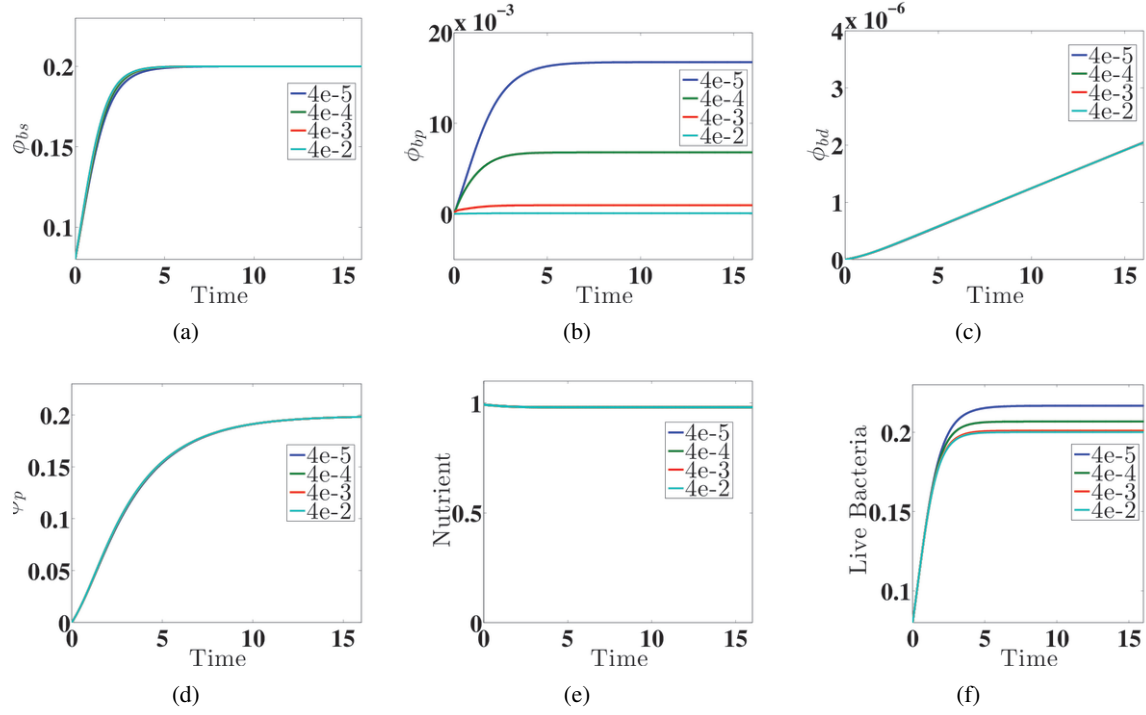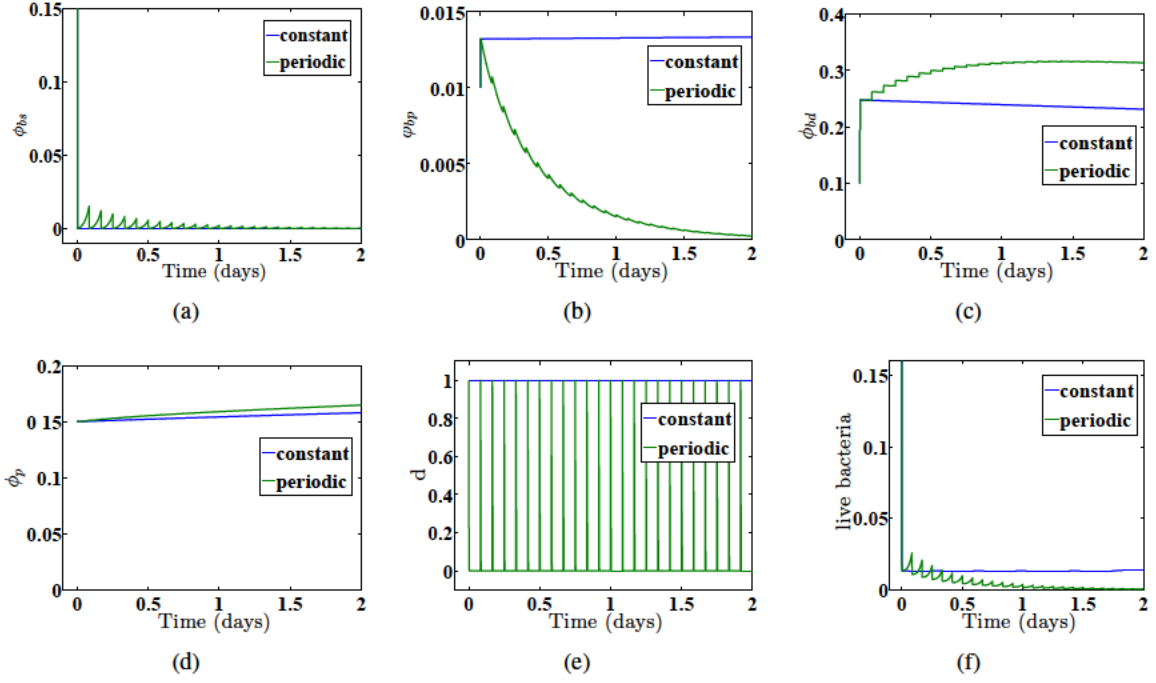
Figure 2: Growth dynamics of spatially homogeneous biofilms. This figure shows biofilm growth dynamics with respect to four selected conversion rates $b_{ps,\max}$: $4 \times 10^{-5}, 4 \times 10^{-4}, 4 \times 10^{-3}, 4 \times 10^{-2}$. The volume fractions of the susceptible, persister, dead bacteria, EPS and the concentration of nutrient and total volume fraction of live bacteria with time are shown in (a)-(d) respectively.

Figure 3: Dynamics of spatially homogeneous biofilms being treated by antimicrobial agents. This figure shows two simulations: one with antimicrobial agents dosed constantly and the other with antimicrobial agents dosed periodically. The former fails to kill the bacteria in the biofilm while the latter can eradicate the bacteria in the biofilm. Here we suppose nutrient is sufficient. The volume fractions of the susceptible, persister, dead bacteria, EPS, the concentration of antimicrobial agents and the volume fraction of live bacteria with time are shown in (a)-(f), respectively.
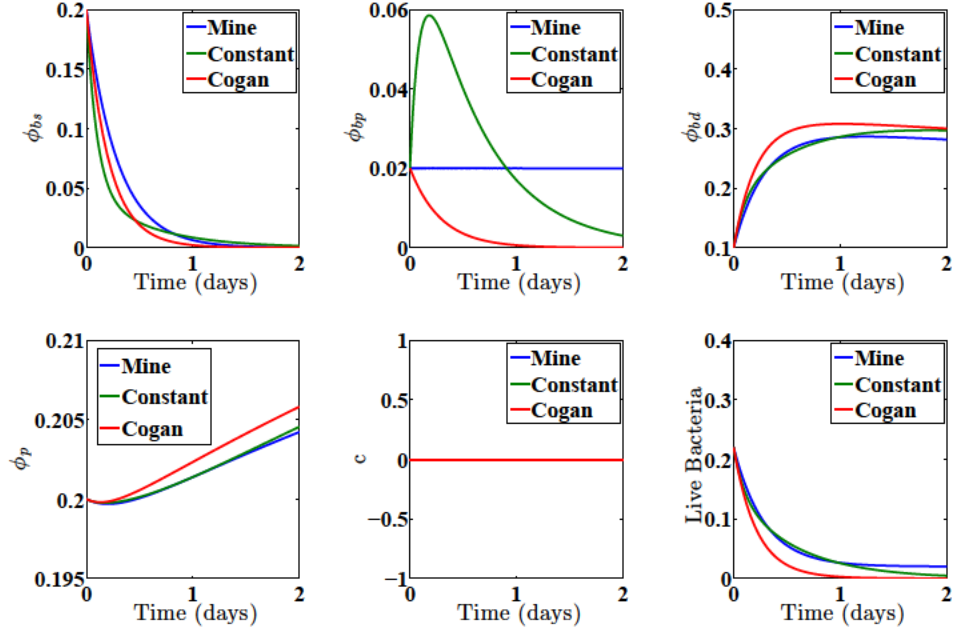
(a) Biofilm growth dynamics with different conversion rates b_{sp}, b_{ps}.
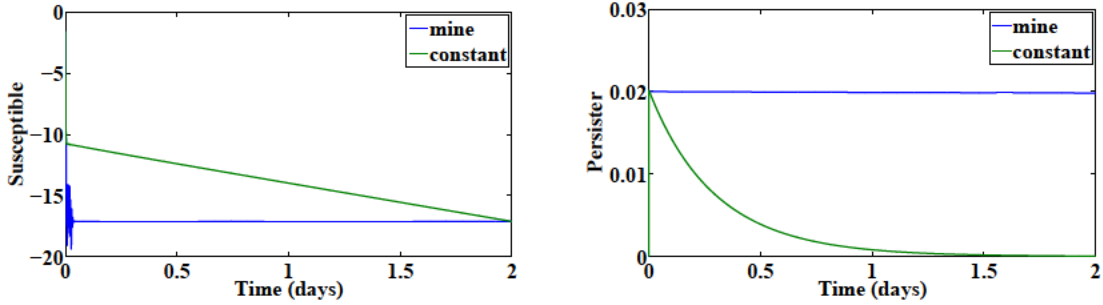
(b) Biofilm dynamics while treated by antimicrobial agents with different conversion rates b_{sp}, b_{ps}.

Figure 4: A Comparison of biofilm growth and dynamics after being treated by antimicrobial agents with different conversion rates b_{sp} and b_{ps}. In this figure, three conversion model for b_{sp} and b_{ps} are used: the constant conversion rates $b_{sp} = b_{sp1}$, $b_{ps} = b_{ps,max}$, the conversion rates of equation (32), where $d_0 = 0.1$, $\varepsilon = 0.01$ and the conversion rates of equation (20), which are represented in the legend by 'Constant', 'Cogan' and 'Mine', respectively. (a) A comparison biofilm growth dynamics when nutrient supply is deficient. (b) A comparison of dynamics for biofilm being treated by antimicrobial agents.
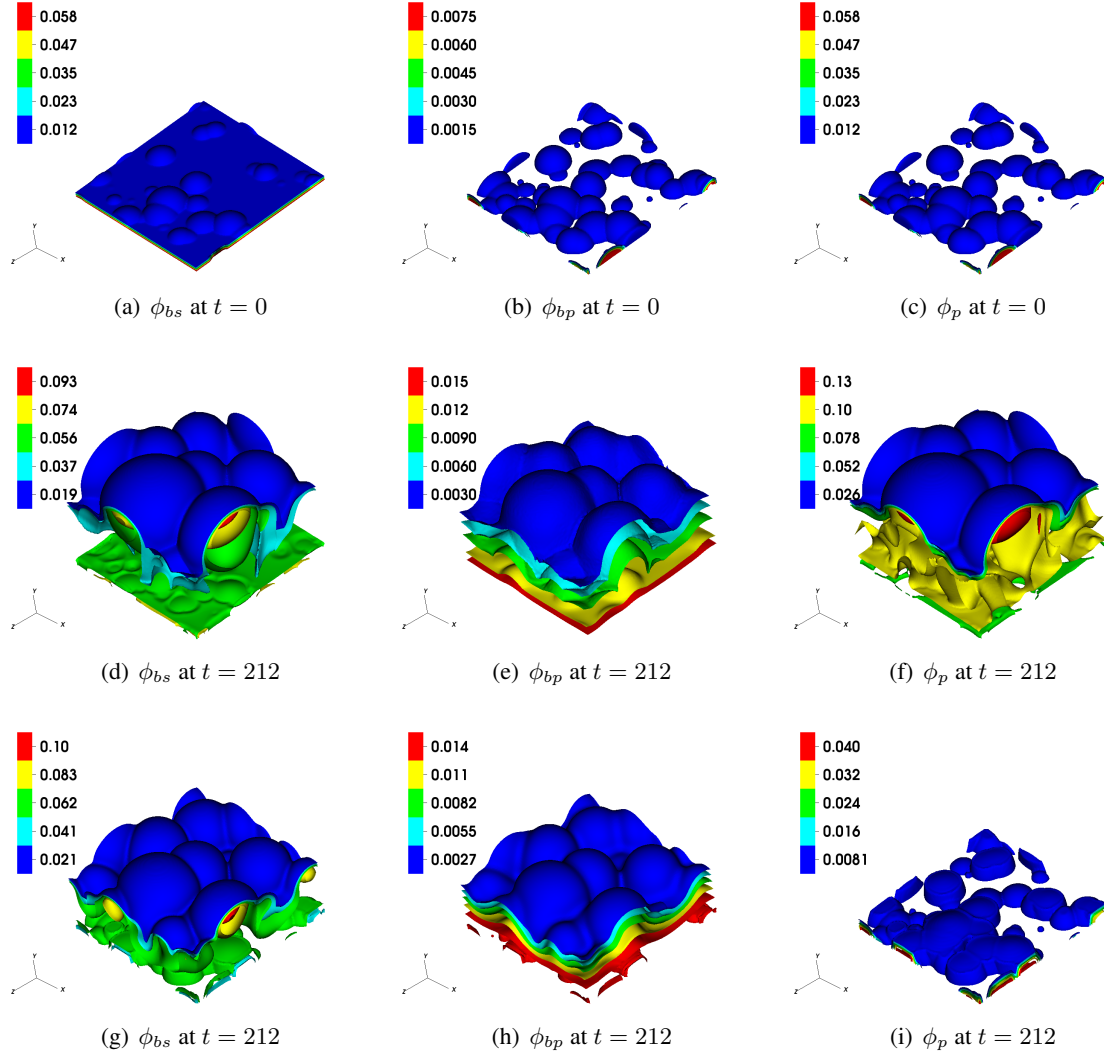
Figure 5: Biofilm development with varying EPS production rates. It shows that enhanced EPS production can expand the biofilm. (a)-(c) initial volume fractions of the susceptible, the persister and EPS; At time $t = 212$, volume fractions of the susceptible, the persister and EPS, when the EPS production rate $C_5 = 8 \times 10^{-4}$, are shown in (d)-(f) respectively; (g)-(i) are the volume fractions of the susceptible, the persister and EPS without EPS prodution ($C_5 = 0$).
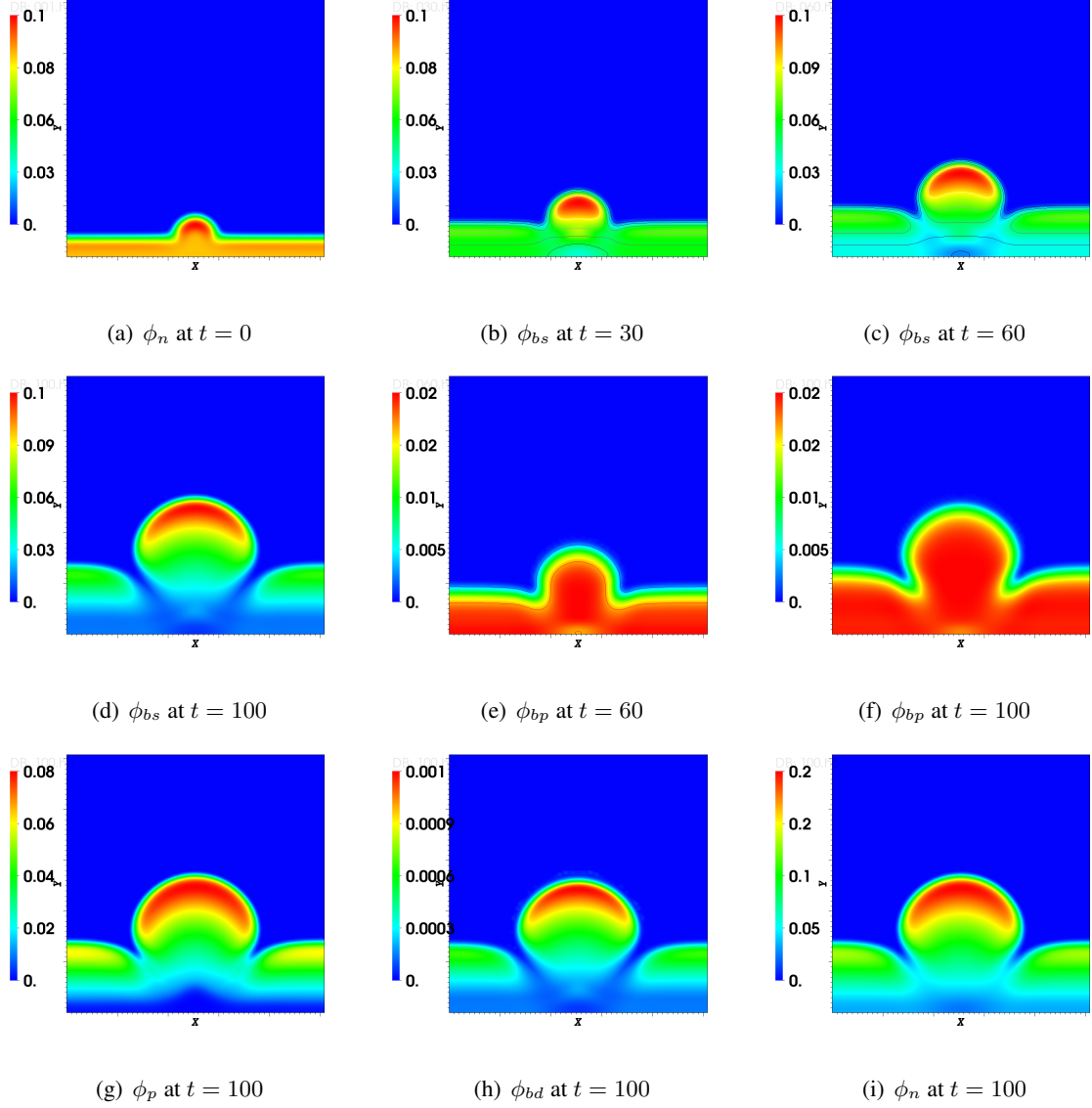
(a) ϕ_n at $t = 0$ (b) ϕ_{bs} at $t = 30$ (c) ϕ_{bs} at $t = 60$

(d) ϕ_{bs} at $t = 100$ (e) ϕ_{bp} at $t = 60$ (f) ϕ_{bp} at $t = 100$

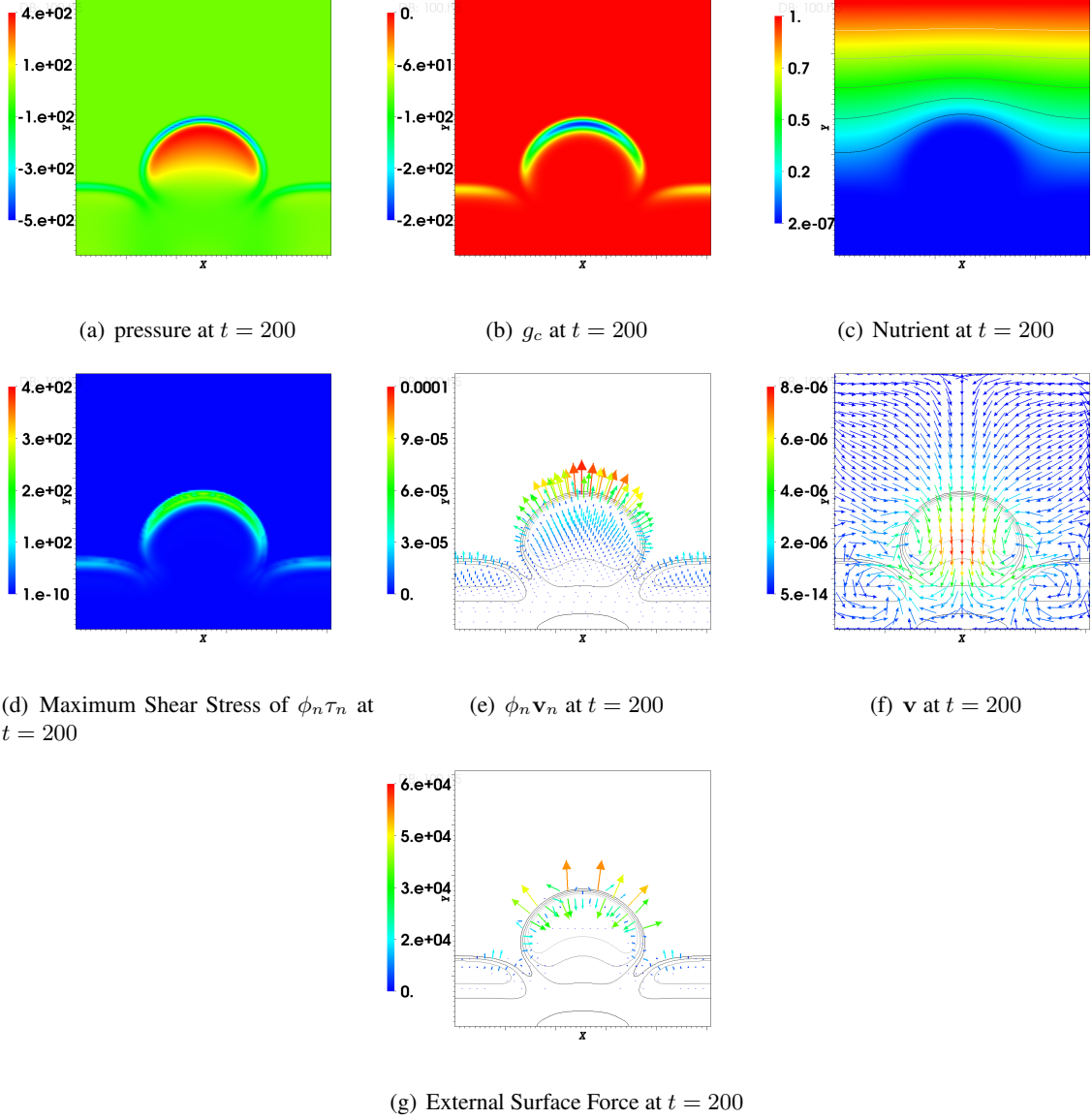(g) ϕ_p at $t = 100$ (h) ϕ_{bd} at $t = 100$ (i) ϕ_n at $t = 100$

Figure 6: Void structures in biofilm colonies due to the death of bacteria as a result of depleted nutrient. This figure shows heterogenous biofilm growth dynamics of a single biofilm bump. In this case, nutrient is supplied on the top and initially there is a single bump containing only susceptible bacteria, where we choose $\phi_{p,\max} = 0.1$, $r_{bd} = 10^{-3}$, $r_{bs} = r_p = 10^{-5}$. In order to depict it clearly, all plots are 2D slices at $z = 0.5$. (a) initial biofilm colony; (b)-(d) volume fraction of susceptible bacteria at $t = 30, 60, 100$ respectively; (e)-(f) volume fraction of persister bacteria at $t = 60, 100$ respectively; (g)-(i) volume fraction of EPS, dead bacteria and total biomass at $t = 100$ correspondingly.

30

(a) pressure at $t = 200$

(b) g_c at $t = 200$

(c) Nutrient at $t = 200$

(d) Maximum Shear Stress of $\phi_n \tau_n$ at $t = 200$

(e) $\phi_n \mathbf{v}_n$ at $t = 200$

(f) $\mathbf{v}$ at $t = 200$

(g) External Surface Force at $t = 200$

Figure 7: Void structures in biofilm colonies due to the death of bacteria as a result of depleted nutrient. This figure shows other 2D slice plots ($z = 0.5$) for simulations in figure 6 at time $t = 200$. (a) hydrodynamic pressure; (b) nutrient consumeption rate; (c) nutrient distribution; (d) maximum shear stress due to biomass; (e) effective biomass flux; (f) volume averaged velocity; (g)external surface force (force derived by least action principle in moment equation).

31
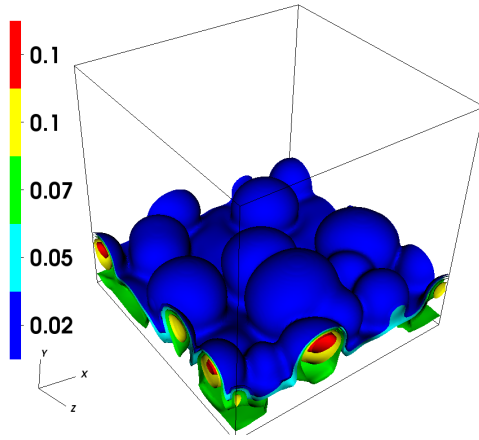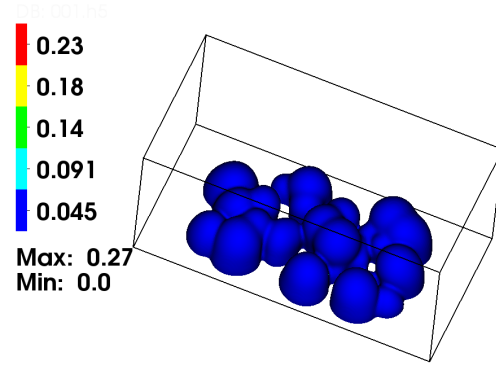
(a) ϕ_n at $t = 0$ (b) ϕ_n at $t = 0$

Figure 8: Initial Condition for later biofilm treatment simulations. This figures show well-grown biofilms, which will be used as initial conditions for later simulations: (a) volume fraction of total biomass for a grown biofilm in an infinite-long channel, where we simply suppose the susceptible, persister and EPS and dead bacteria has same distribution with volume fraction ratio as $3 : 1 : 1 : 0$; (b) grown biofilm in a water tube, where the corresponding ratios are proposed as $1 : 1.2 : 0 : 0$.

(a) ϕ_{bs} at $t = 10$

(b) ϕ_{bs} at $t = 26$

(c) ϕ_{bs} at $t = 134$

(d) ϕ_{bs} at $t = 0$

(e) ϕ_{bs} at $t = 10$

(f) d at $t = 134$

(g) ϕ_{bd} at $t = 134$

(h) ϕ_{bp} at $t = 134$

(i) ϕ_{p} at $t = 134$
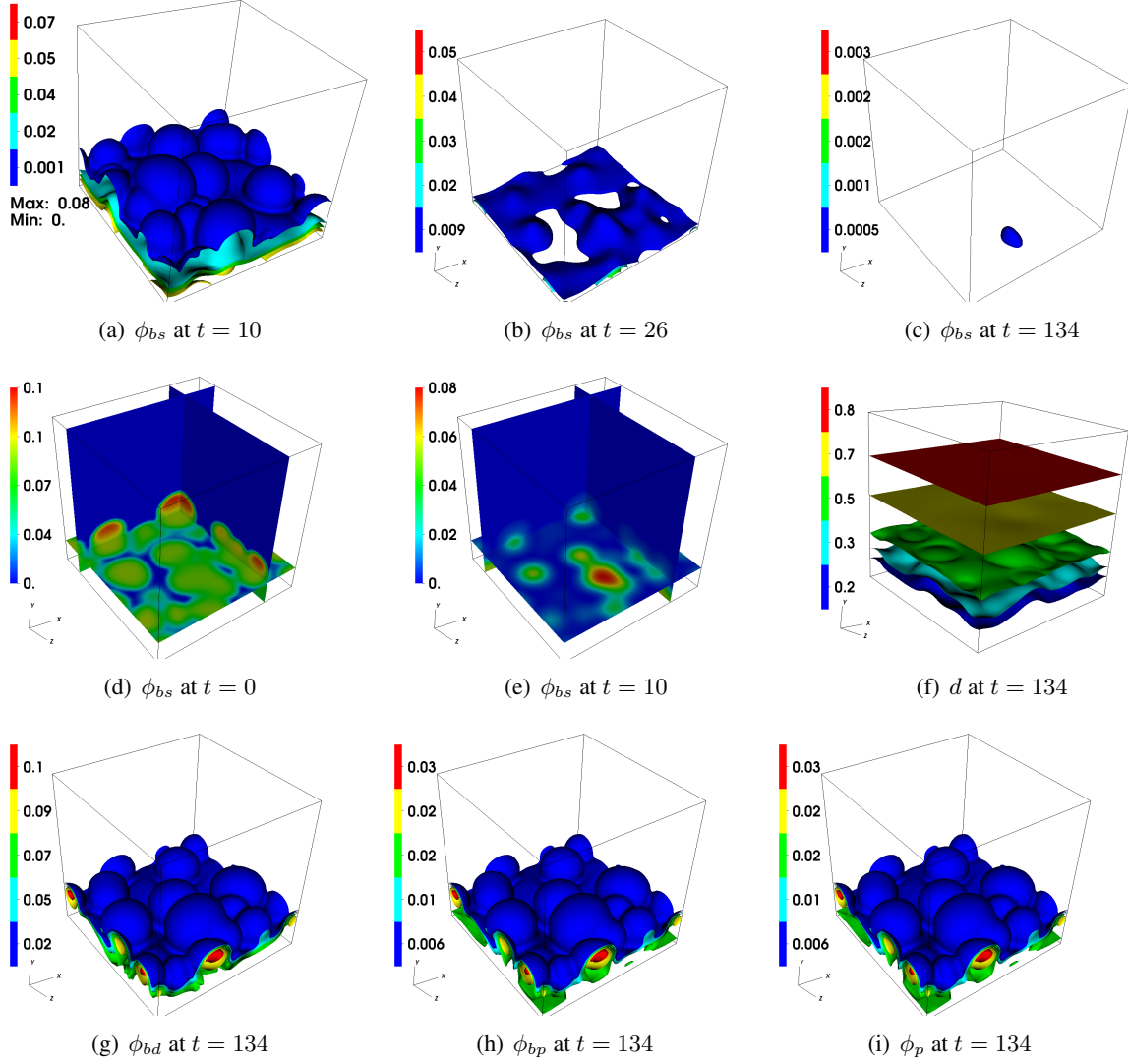
Figure 9: Antimicrobial treatment process in an infinite-long channel using well-mixed antimicrobial agents dosed from the top boundary. This figure shows susceptible bacteria are dramatically eradicated, leaving only persister cells: (a)-(c) susceptible bacteria volume fraction at time $t = 10, 36, 134$ respectively; (g)-(e) three slices of susceptible bacteria at $t = 0, 10$ correspondingly; (f) antimicrobial agent concentration at $t = 134$ (g)-(i) dead bacteria and persister and EPS at $t = 134$, respectively.

(a) ϕ_{bs} at $t = 2$

(b) ϕ_{bs} at $t = 14$

(c) ϕ_{bs} at $t = 24$

(d) ϕ_{bp} at $t = 2$

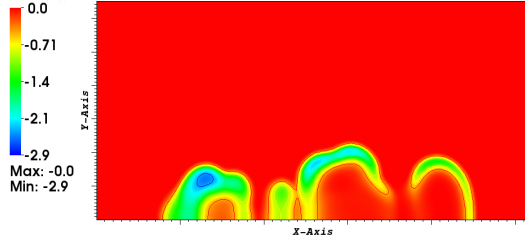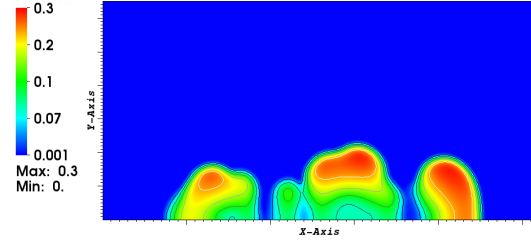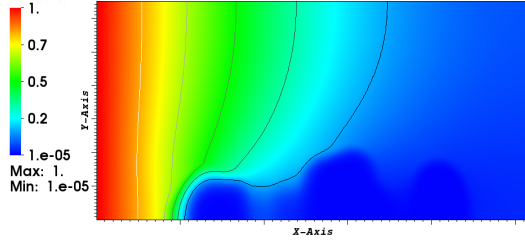(e) ϕ_{bp} at $t = 24$

(f) ϕ_{bd} at $t = 24$
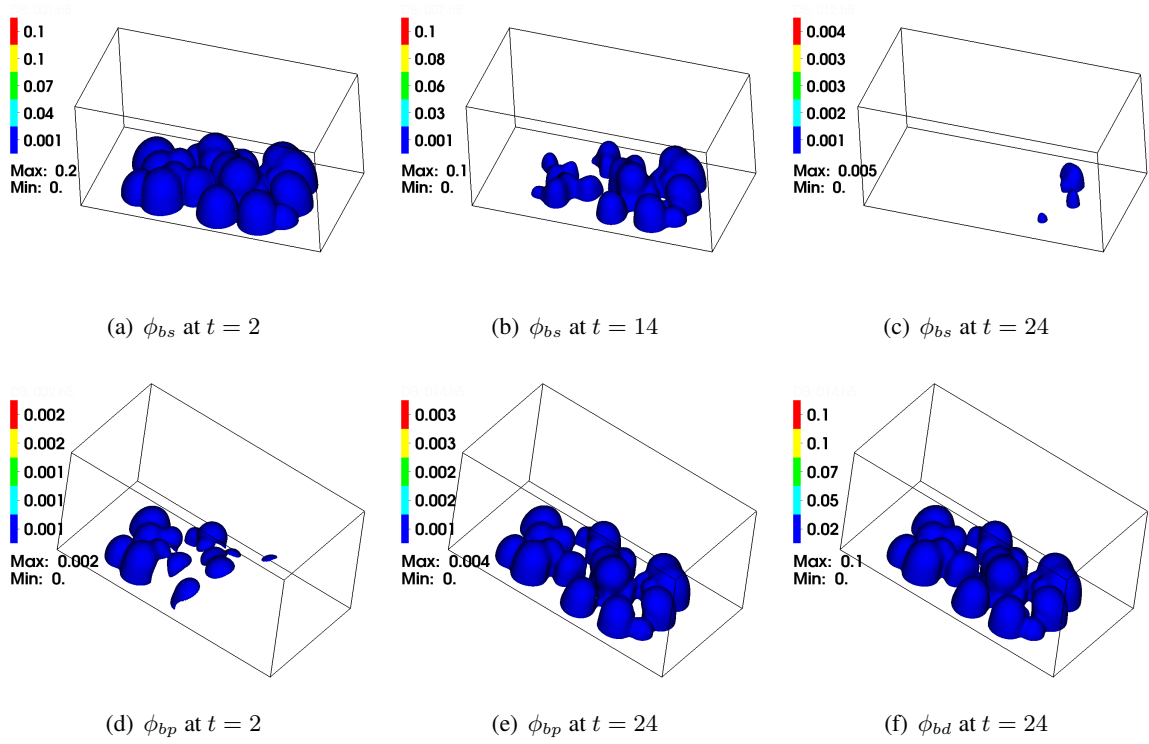
Figure 10: Biofilm treatment in a finite-long tube using well-mixed antimicrobial agents dosed from inlet boundary. Here the reference time is $t_0 = 10$ seconds and the initial biofilm colony is shown in figure 8(b). (a)-(c) the volume fraction of susceptible bacteria at time $t = 2, 14, 24$, respectively; (d)-(e) the volume fraction of persister bacteria at $t = 2, 24$ respectively; (f) the volume fraction of dead bacteria at $t = 24$.
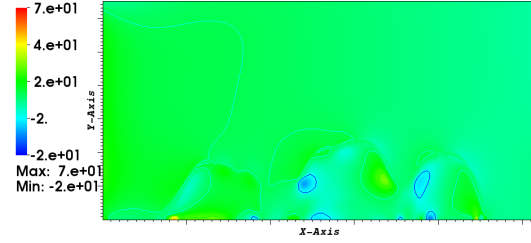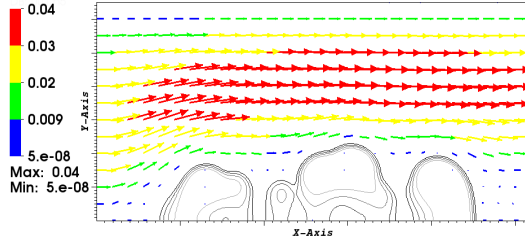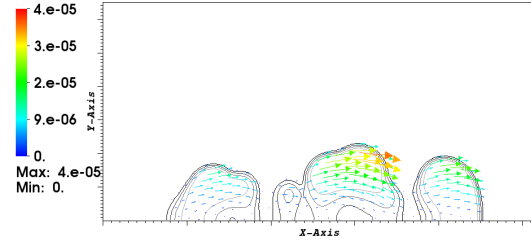
(a) g_d at $t = 2$

(b) Total Biomass at $t = 2$

(c) Concentration of Antimicrobial Agent at $t = 2$

(d) Effective Hydrodynamic Presure at $t = 2$

(e) $\mathbf{v}$ at $t = 2$

(f) $\phi_n \mathbf{v}_n$ at $t = 2$

Figure 11: Biofilm treatment in a finite-long tube using well-mixed antimicrobial agents dosed from inlet boundary. This figure shows 2D slice ($z = 0.5$) for the simulation in figure 10 at time $t = 2$. (a)antimicrobial agent consumption rate; (b) total biomass distribution; (c) antimicrobial agent distribution; (d) hydrodynamic press; (e) volume-averaged velocity; (f) biomass flux.

(a) ϕ_{bd} at $t = 124$

(b) ϕ_{bd} at $t = 310$

(c) ϕ_{bd} at $t = 1463$

(d) d at $t = 310$

(e) ϕ_{bs} at $t = 1463$

(f) ϕ_{bp} at $t = 1463$
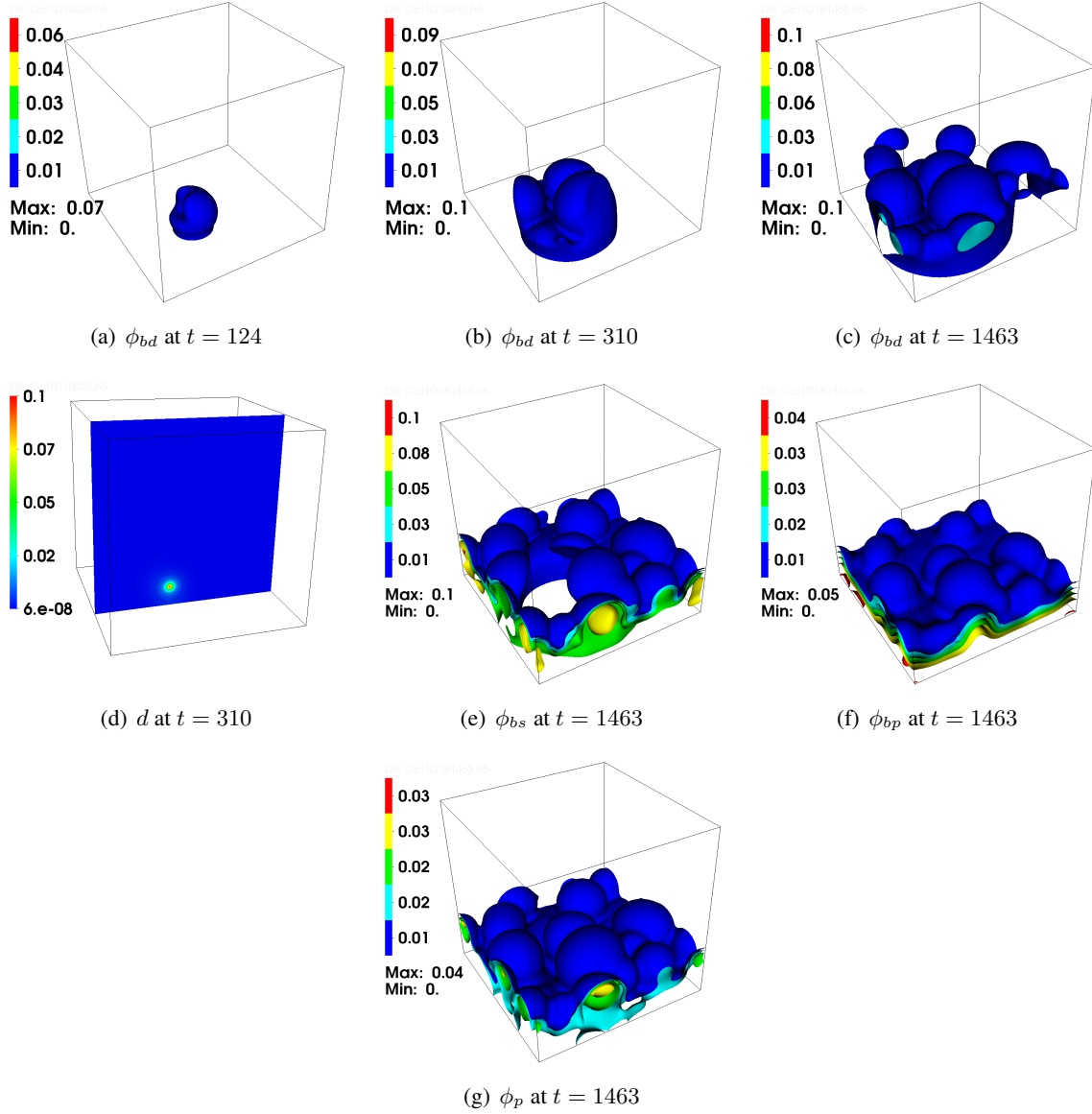
(g) ϕ_p at $t = 1463$

Figure 12: Biofilm treatment by antimicrobial agents injected through an injection needle. A highly heterogeneous distribution of dead bacteria is observed due to the pinpointed dosing strategy. The initial profiles is given in figure 8(a) and the injection position is chosen as $(0.6, 0.1, 0.4)$. (a)-(c) provides the profiles of dead bacteria at varying time: $t = 124$, 310, 1463, respectively; (d) 2D slice ($z = 0.4$) of concentration of antimicrobial agents at $t = 310$; the volume fractions of the susceptible, the persister and EPS at time $t = 1463$ are given in (e)-(g), respectively.

(a) ϕ_{bs} at $t = 76$

(b) ϕ_{bs} at $t = 190$

(c) ϕ_{bs} at $= 235$

(d) ϕ_{bd} at $t = 235$

(e) ϕ_{bp} at $= 235$

(f) ϕ_{p} at $= 235$

(g) ϕ_{bs} at $= 235$

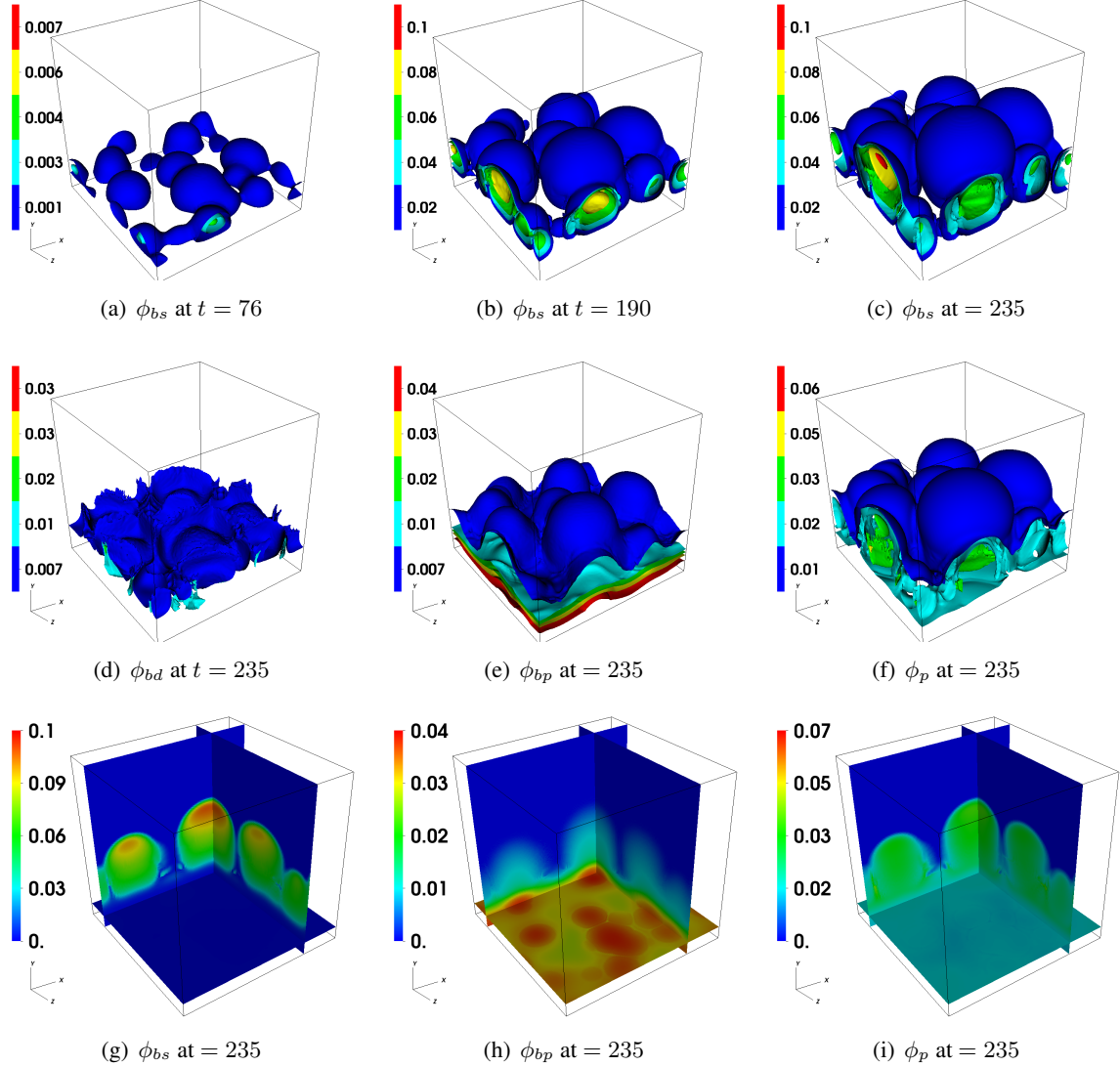(h) ϕ_{bp} at $= 235$

(i) ϕ_{p} at $= 235$

Figure 13: Biofilm relapse after the cessation of an antimicrobial agents dosing. The biofilm is observed to relapse as susceptible bacteria regrow into colonies due to the persister-susceptible conversion after the treatment. The initial biofilm colony is an antimicrobial-treated one taken from the numerical experiment in Figure 9, where all the susceptible bacteria are eradicated. (a)-(c) shows susceptible bacteria at time $t = 76, 190, 235$ respectively; (d)-(f) shows the volume fractions of dead bacteria, the persister and EPS at $t = 235$ correspondingly; (g)-(i) shows three slices of the volume fractions for the susceptible, persister bacteria and EPS at $t = 235$ respectively.

(a) ϕ_{bs} at $t = 10$ (b) ϕ_{bs} at $t = 10$ (c) ϕ_{bs} at $t = 10$

(d) ϕ_{bs} at $t = 30$ (e) ϕ_{bs} at $t = 30$ (f) ϕ_{bs} at $t = 30$
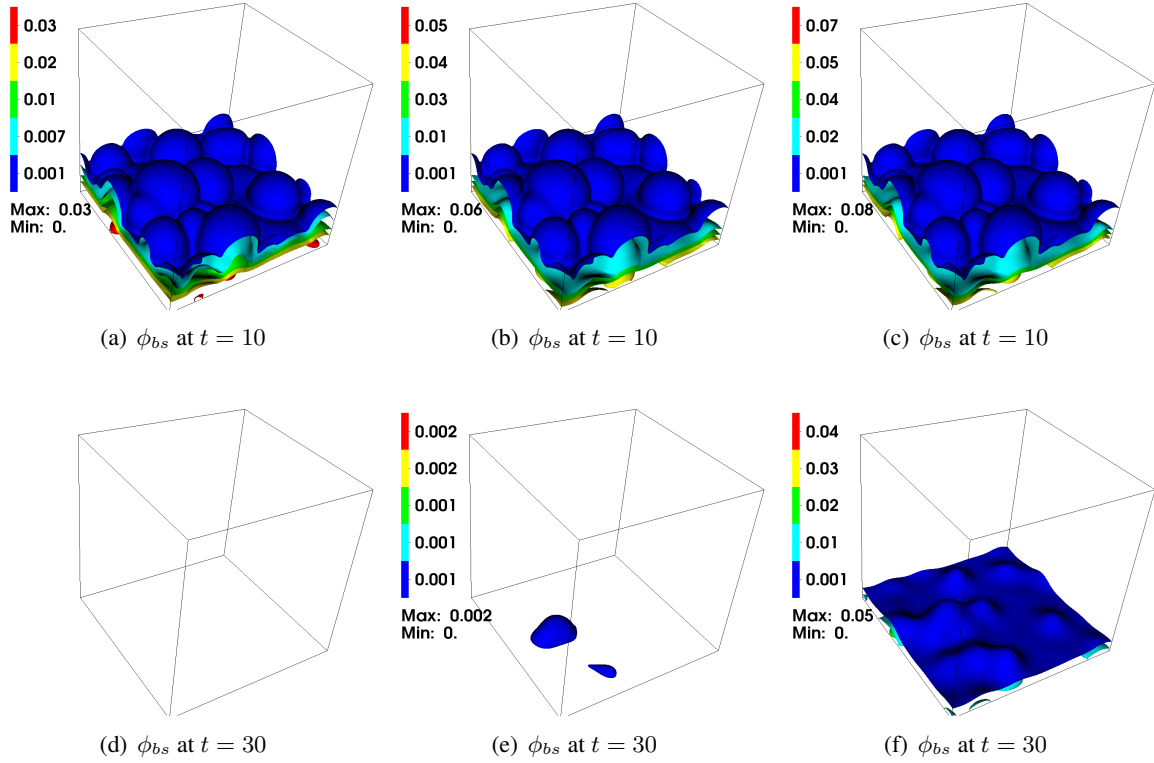
Figure 14: A comparison of varying antimicrobial diffusion rates in a disinfection process. This figure shows antibiotic treatment of biofilms in an infinite-long channel with antimicrobial agents dosed on the upper boundary, using three different diffusion rates: D_{e1}, D_{e2} and D_{e3}. The initial condition is shown in Figure 8(a). The volume fraction of the susceptible bacteria for penetrating rates D_{e1}, D_{e2} and D_{e3} at $t = 10$ are shown in (a)-(c) respectively; and (d)-(f) shows the corresponding volume fractions of the susceptible bacteria at $t = 30$.
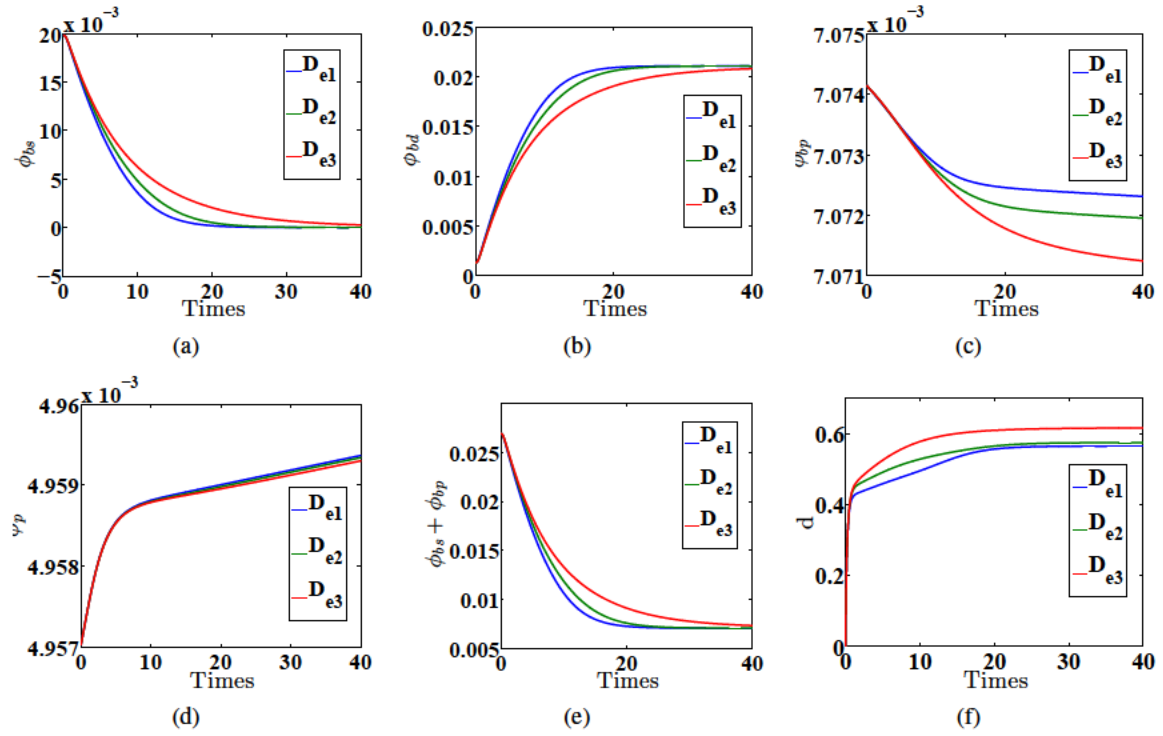
Figure 15: A comparison of varying antimicrobial diffusion rates in a disinfection process. This figure shows total volume fractions of each components for simulations in figure 14: (a)-(d) total volume fractions of susceptible, dead, persister bacteria and EPS, correspondingly; (e) total volume fraction of live bacteria; (f) total concentration of antimicrobial agents.

(a) ϕ_{bp} at $t = 212$

(b) ϕ_{bp} at $t = 1098$

(c) ϕ_{bp} at $t = 1782$

(d) ϕ_{bs} at $t = 1782$

(e) ϕ_{bd} at $t = 1782$
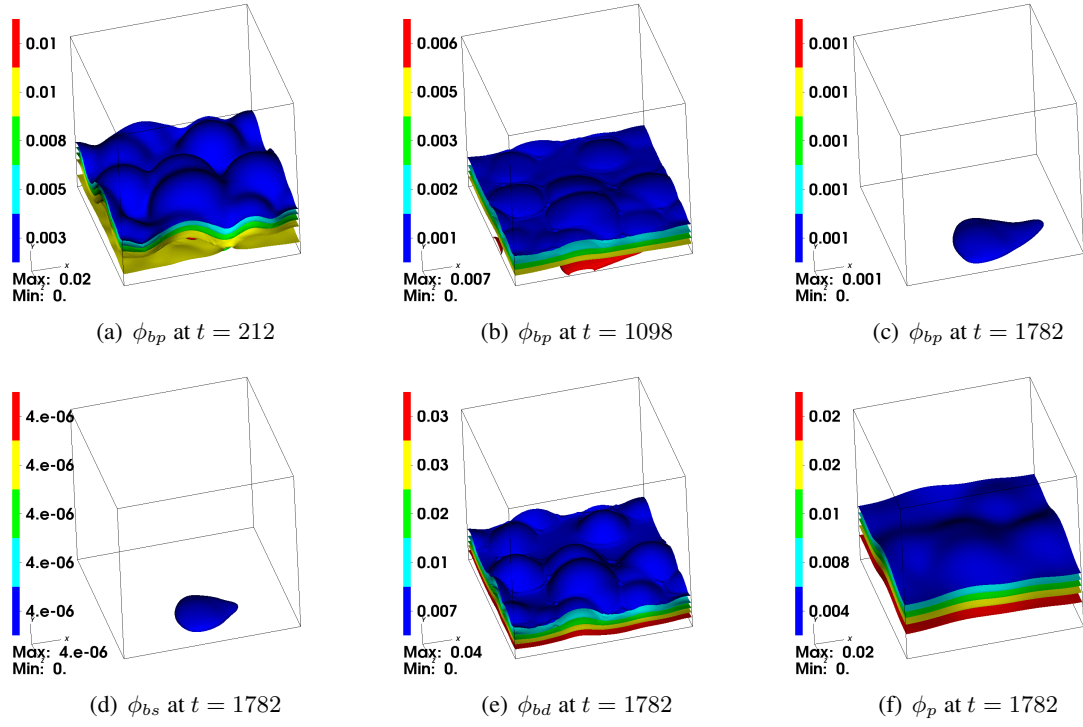
(f) ϕ_p at $t = 1782$

Figure 16: Periodic dosing strategies succeed in treating biofilms. Given a well-grown biofilm from figure 8(a), antimicrobial agents are dosed periodically. Then, the live bacteria are gradually eradicated. The volume fraction of persister bacteria at varying times: $t = 212, 1098, 1782$ are shown in (a)-(c) respectively; (d)-(f) shows the volume fractions for the susceptible, dead bacteria and EPS, correspondingly.